

The Hitchhiker’s Guide to Programming and Optimizing CXL-Based Heterogeneous Systems

Zixuan Wang[‡], Suyash Mahar[‡], Luyi Li[‡],
 Jangseon Park^{‡*}, Jinpyo Kim^{‡*}, Theodore Michailidis[‡], Yue Pan[‡],
 Tajana Rosing[‡], Dean Tullsen[‡], Steven Swanson[‡],
 Kyung Chang Ryoo^{*}, Sungjoo Park^{*}, and Jishen Zhao[‡]

[‡]University of California San Diego ^{*}Samsung ^{*}SK Hynix

Abstract

We present a thorough analysis of the use of CXL-based heterogeneous systems. We built a cluster of server systems that combines different vendor’s CPUs and various types of CXL devices. We further developed a heterogeneous memory benchmark suite, HEIMDALL, to profile the performance of such heterogeneous systems. By leveraging HEIMDALL, we unveiled the detailed architecture design in these systems, drew observations on optimizing performance for workloads, and pointed out directions for future development of CXL-based heterogeneous systems.

1 Introduction

The ever-growing performance demands from modern applications drive the development of heterogeneous systems. However, heterogeneous systems’ communication bandwidth has become one of the key bottlenecks in system scalability, where the hardware bandwidth does not scale as fast as modern workloads’ bandwidth requirements. To improve the bandwidth, devices such as network cards and GPUs have developed dedicated communication links [1] to exchange data more efficiently. However, such new communication links often define their own communication protocols, requiring specialized operating system kernel drivers and system software libraries and imposing new programming models on workload developers. Adding such new devices to an existing heterogeneous system is thus non-trivial, which can hold back their adoption. This motivates the need for an industry-standard communication protocol to provide a consistent interface to workloads while enabling device manufacturers to integrate new devices into the ecosystem without changing the programming interface.

Cache coherent interconnect protocols are proposed to unify the communication interface between heterogeneous devices. Using cache-coherent interconnects, processors can access data through connected processors and cache the remote data locally; at the same time, the protocol transparently updates the locally cached data when modified by any connected processor. Such protocols allow processors to exchange data in a single standard scheme, simplifying data synchronization and reducing the use of dedicated communication drivers and libraries. Many existing cache coherent protocols are initially deployed for homogeneous systems, such as inter-CPU links (Intel UPI [2], and AMD Infinity Fabric [3]). With the rapid emergence of new processors and memory devices, industry and academia have been exploring generic cache coherent links [4–7] for heterogeneous systems to interconnect different types of processors and memory. Such generic protocols aim to unify communication schemes and optimize data exchange performance between devices.

Compute Express Link [4] (CXL) is a recent open standard of cache coherent interconnect protocol and has been commercially supported in its early stage. CXL defined an multi-device coherence protocol on-top-of PCIe physical layer, allowing processors to reuse the existing PCIe standard (links, form factors, and more) as much as possible instead of adopting a new physical layer design. When interconnected with CXL, accelerators and memory devices can sit on the PCIe bus and exchange data coherently with other devices, including the host CPU. As of today, CXL has three generations of standard specs, from 1.0 to 3.0. The CXL 1.0 spec lays the foundation of CXL standard, defining

the basics of coherence and device data exchange protocols; the later revised 1.1 spec added the spec for the memory expander devices. The CXL 2.0 introduced switch-based topologies, enabling scalable multi-device configurations and improved memory pooling. The recent CXL 3.0 doubled the bandwidth with PCIe Gen 6 and incorporated advanced features such as atomic operations and enhanced security, supporting more demanding applications like AI and large-scale memory pools.

To study the CXL systems’ performance characteristics, we first built a cluster of CXL-based heterogeneous systems that combine various CPUs and CXL memory devices. We chose two types of CPUs, Intel Sapphire Rapids (SPR) and AMD Genoa (Zen4) for our machines, given their different capabilities: The Intel-SPR CPU implements CXL 1.0 standard, supports Intel FPGA-based CXL Type 1 and 2 devices through CPU firmware, and emulates the CXL.mem through CXL.cache interface. The AMD-Zen4 CPU implements CXL 1.1 standard with native supports of CXL.mem interface. We then incorporated two categories of CXL devices, FPGA-based and ASIC-based: We implemented CXL Type 1, Type 2, and Type 3 devices based on Intel Agilex 7 FPGAs and integrated them with Intel-SPR CPUs. Additionally, we incorporated ASIC-based CXL memory expanders to both Intel and AMD CPUs.

We then studied the performance characteristics in such heterogeneous systems, compared performance metrics side-by-side across different systems, and drew observations. To this end, we developed a benchmark suite, HEIMDALL, and leveraged it to conduct a wide range of performance profiling. This benchmark suite consists of carefully crafted microbenchmarks that trigger specific system behaviors across system layers, from microarchitecture to operating systems levels. By analyzing the benchmark result on a single system, we observed characteristics such as CPU and CXL device microarchitecture designs that support the CXL protocol, together with OS and system software performance, while leveraging CXL devices. Then by comparing benchmark results across systems, we observed discrepancies between systems, including different CPU-side CXL designs between AMD and Intel and device-side architectural implications for performance.

In summary, we make the following contributions:

- We built a cluster of CXL-based systems and summarized our lessons learned throughout this process.
- We developed a benchmark suite—HEIMDALL—for heterogeneous memory systems.
- By leveraging this benchmark suite, we studied a wide range of CXL-based heterogeneous system configurations in our cluster and uncovered CXL-related architecture and system designs.
- We draw key observations from our extensive experiments and point out future directions in developing CXL-based heterogeneous systems.
- We have a list of works undergoing and will update this paper in the future to include power analysis, CXL FPGA internals, the latest CXL prototypes’ performance, and more.

2 Background and Methodology

2.1 Compute Express Link (CXL)

Compute Express Link (CXL) [4] is an open industry-standard interconnection protocol designed to facilitate high-speed communications between processors, accelerators (such as GPUs and SmartNICs), and memory devices in computing systems. A unique feature of CXL is its capability at the hardware level to enable coherent memory access across heterogeneous architectures. This coherence ensures that various processors and accelerators can transparently share memory resources as though they were part of a unified system. By leveraging CXL, we can simplify the memory access operations in heterogeneous programming models.

2.1.1 CXL Protocol and Device Types

CXL supports three different protocols: CXL.io, CXL.cache, and CXL.mem. CXL.io is identical to the PCIe protocol and enables device discovery, enumeration, and PCIe IO transactions. On the other hand, CXL.cache and CXL.mem enable coherent cache communication among devices. CXL.mem allows the host to coherently access device memory, and CXL.cache additionally allows the device to coherently cache host memory on the device.

CXL defines three device types, Type 1 to 3, as shown in Figure 1, for different use cases: Type 1 devices are traditional PCIe devices and support only the CXL.cache protocol. Type 2 devices are accelerators with onboard memory (e.g.,

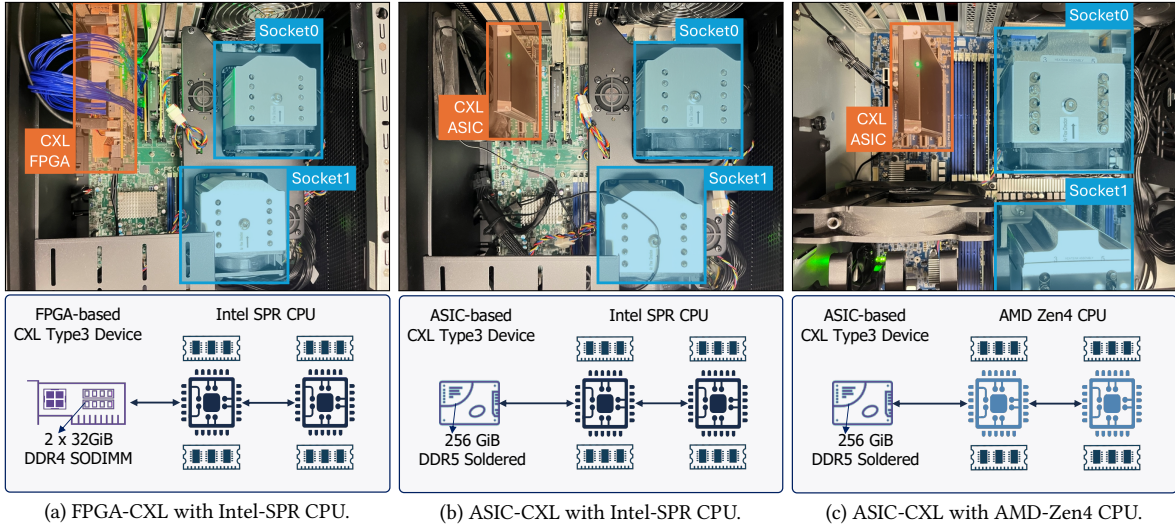


Figure 1: CXL system organization overview, the top sub-figures are photos of the real machine we’ve built, and the bottom sub-figures are illustration of system build.

GPUs) and support all three CXL protocols. Finally, Type 3 devices have onboard memory for capacity and bandwidth expansion but do not cache host memory; they support CXL.io and CXL.mem.

The CXL systems we tested provide three types of interfaces to access the CXL on-device resources: (1) All of our CXL devices expose PCIe interfaces—such as PCIe config space and user-defined memory-mapped registers—for configuring CXL device behaviors. Type 1 and 2 devices expose an additional PCIe interface for programs to interact with on-device accelerators. (2) Type 2 and 3 devices enumerate their on-device memory as an additional NUMA memory node for programs to access such memory. This ensures any existing workload can easily use CXL memory through the NUMA interface instead of specialized libraries. (3) Selectively, type 2 and 3 devices can be configured to expose their memory as a Direct Access (DAX) file—a memory-mapped device file in Linux systems—allowing workloads to use `mmap()` to access CXL memory. Once enabled, this DAX mode removes the corresponding amount of memory from the NUMA memory node to prevent conflict access from both sides.

2.1.2 CXL Enumeration

To boot a system with CXL devices, CPU firmware and operating system kernel have to support CXL. CXL device enumeration is the process where the BIOS/UEFI and OS discover and identify devices connected to the CXL bus. This process is required to establish communication between the host CPU and CXL devices.

During the early bootup stage, the BIOS/UEFI automatically probes all devices connected to the PCIe (including CXL devices) and establishes early communication with CXL devices. Different CPUs handle this process differently. For example, our Intel-SPR CPUs can fully enumerate the Intel-FPGA-based CXL devices without the help of the OS kernel, while our AMD CPUs cannot correctly enumerate the FPGA-based devices. CPU vendors can implement dedicated CXL enumeration processes for their CXL products (which may have specialized designs such as accelerator communication protocols and device IDs), leaving the OS kernel to enumerate generic CXL devices that comply with CXL standards. We found our Intel-SPR CPU using the specialized PCIe device ID (0x0ddb) provided by Intel CXL FPGA to identify such devices and properly enumerate them, while our AMD CPUs do not recognize such ID.

After BIOS/UEFI finishes booting, the OS kernel (the Linux kernel in our paper) takes over and relies on its CXL device driver to further set up CXL devices. This process includes discovering CXL devices from PCIe devices, extracting CXL-related information from config registers (such as CXL-attached memory size and start address), creating corresponding Linux device files, and adding a new NUMA node for CXL-attached memory, if any. The Linux kernel support for CXL is still under development and refinement, and only until Linux 6.8-rc2 does it correctly recognize Intel FPGA-based Type 3 devices [8], and more supports coming under the path.

Table 1: System Specifications.

Category	Specification	Details
Intel-SPR	Processor	2 × Intel Xeon Silver 4416+
	Architecture	Sapphire Rapids (SPR)
	Cores/Threads	40/80
	L1i Cache	32 KiB per core
	L1d Cache	48 KiB per core
	L2 Cache	2 MiB per core
	L3 Cache	38 MiB per socket
	Main Memory	8 × 32 GiB DDR5 DIMMs
	CXL Support	CXL 1.1 with native supports for type 1 and type 2
AMD-Zen4	Processor	2 × AMD EPYC 9124
	Architecture	Zen4
	Cores/Threads	32/64
	L1i Cache	32 KiB per core
	L1d Cache	32 KiB per core
	L2 Cache	1 MiB per core
	L3 Cache	16 MiB per 4 cores
	Main Memory	8 × 16 GiB DDR5 DIMMs
	CXL Support	CXL 1.1+ with native supports for type 1, 2 and 3
FPGA-CXL	Memory Capacity	64 GiB
	Memory Media	2 × 32GiB DDR4 SODIMMs
Memory Expander (ASIC-CXL)	Memory Capacity	256 GiB
	Memory Media	Soldered DDR5 modules
Software	Linux kernel	6.9
	Intel Quartus	2023.4

2.2 Accessing CXL Resources

There are three types of CXL devices with different combinations of CXL resources. Type 1 devices are pure accelerator devices without memory exposed to host CPUs. Type 3 devices are pure memory devices without exposing any accelerator to host CPUs. Type 2 provides both accelerator and memory resources for the host.

To access CXL accelerator resources provided by Type 1 and Type 2, a program communicates with the CXL’s PCIe device file provided by the Linux kernel and follows the accelerator’s communication protocol. To access CXL memory resources provided by Type 2 and Type 3, a program can choose to access through NUMA interface or a direct-access (DAX) device file. CXL memory is by default exposed as an additional NUMA memory node in the Linux system, allowing any program to easily access it through NUMA libraries or the `numactl` command line tool. Selectively, users or programs can configure the device to expose CXL memory through a DAX device file through the `daxctl` command line tool. Once configured, the program can use the `mmap()` system call to map this DAX file into its address space and then directly manage this memory space. Any access through such a DAX file will directly access the CXL memory without any DRAM memory as an intermediate cache. Such a method gives the program more flexibility in managing CXL memory space [9].

2.3 System Description and Experimental Configurations

As listed in Table 1, we built our cluster with two types of CPUs and two types of CXL devices. We employ Intel Sapphire Rapids 4416+ CPUs, which implement the CXL 1.1 interface [10], support Intel-FPGA-based Type 1 and Type 2 device enumerations, and support the Type 3 device through the CXL.cache interface. We also deploy AMD Geona 9124 CPUs, which implement CXL 1.1+ interface with native support for CXL Type3 devices through CXL.mem [11]. On the device side, we integrate ASIC-based memory expanders with 256 GiB DDR5 DRAM and evaluate them with both Intel and AMD CPUs. We also implemented all three types of CXL devices on Intel Agilex 7 FPGAs with 64 GiB DDR4 DRAM and evaluated them with Intel CPUs. Unless otherwise stated, we use FPGA Type 3 devices in

our performance evaluations to compare with the ASIC-based memory expander. We utilize the Intel Quartus FPGA Development Kit 2023.4 version for FPGA development. We build Linux 6.9 kernel with the latest CXL supports, including the support for Intel FPGA-based Type 3 devices [8].

2.4 HEIMDALL Framework

HEIMDALL comes with a large set of benchmarks and profiling tools to profile the system performance. This section provides an overview of such components, leaving more detailed descriptions for later sections.

Microbenchmarks. We develop a wide range of microbenchmarks to study the performance at the hardware and microarchitecture level. These microbenchmarks are implemented to trigger specific hardware behaviors; thus, we detect microarchitecture designs by monitoring their performance results under different configurations. As an example, we utilize our pointer-chasing microbenchmarks to study memory latency, and by varying pointer-chasing configurations, we reverse-engineer the memory architecture such as memory controller design and CXL data path. To ensure HEIMDALL microbenchmarks behave as expected, we implement their core functionalities in raw x86 assembly code to rule out potential compiler optimizations.

Application benchmarks. We integrate application-level benchmarks into HEIMDALL to study the system and software performance. We configure these benchmarks to run on various hardware system settings, such as remote vs. local memory access, various memory interleaving schemes, and different sub-NUMA clustering modes. By profiling such benchmarks, we observe the system performance limitations and highlight future directions for performance improvements.

Profiling framework. We develop HEIMDALL as a low-noise profiling framework that runs microbenchmark code in Linux kernel space to access physical memory at low noise. We utilize system configuration tools to reduce noises, including turning off CPU hardware prefetchers, disabling simultaneous multithreading (SMT), disabling interrupt handlers while running microbenchmarks, and boosting CPUs to performance mode through the CPU scaling governor. We adopt profiling tools—such as `perf` [12], AMD `uProf` [13], Intel `PCM` [14]—to collect hardware performance counters.

Open source. We open source HEIMDALL at `github.com/awesome-cx1/` to facilitate future memory system research.

3 Basic Performance

We leverage our HEIMDALL’s microbenchmark suite to study the basic performance characteristics of the CXL memory devices and compare the results with CPU-attached DDR5 DIMMs. We start with the latency and bandwidth measurements, followed by specific instructions’ behaviors, including cacheline flush, prefetch, and atomic instructions. Our key observations in this measurement motivate our further investigation at the micro-architecture layer (Section 4) and application layer (Section 6).

3.1 Load/Store Latency

In the first benchmark, we study the load and store instruction latencies on the two systems using HEIMDALL’s pointer-chasing microbenchmark with temporal (i.e., cacheable) memory loads and stores. We configure the experiment to access at least 32 GiB of memory in pointer-chasing to beat the CPU cache and measure the average access latency, reflecting the memory access latency. Figure 2a and Figure 2b show our results accessing main memory (CPU-attached DDR5 DIMMs) and CXL memory.

Load Latency: As shown in Figure 2a, the CXL memory expander has a consistently higher latency than DRAM DIMMs, at $1.92\times$ to $2.06\times$ higher latency on Intel-SPR and AMD-Zen4 CPUs, respectively, and FPGA-CXL incurs the highest latency among these memory modules. Although CXL memory is expected to perform slower than CPU-attached DIMMs, we find that the CPU memory controller further affects the performance: We observe that Intel-SPR CPU has lower latency than AMD-Zen4 when using the same ASIC-CXL. This indicates that Intel-SPR CPU has a

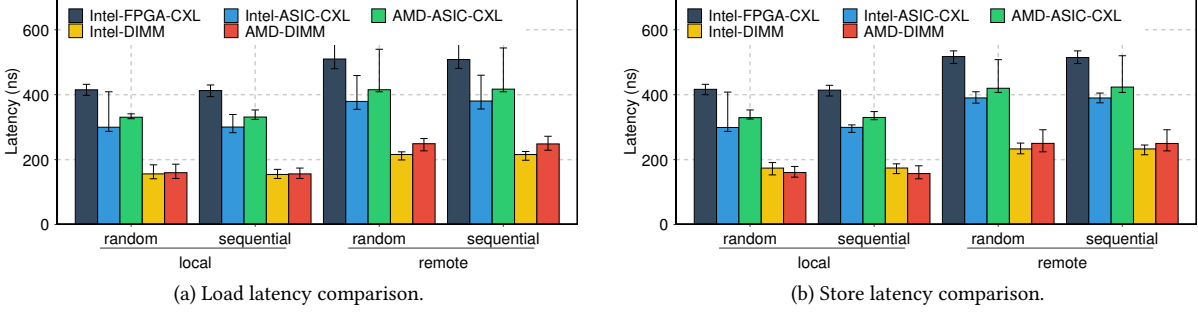


Figure 2: Load and store latency using the pointer-chasing pattern using temporal memory access, with `clflush` after each load and store instruction to enforce access to the off-core memory. The x-axis represents the access pattern (*sequential* or *random*) and access type (accessing memory from *local* NUMA CPU or *remote* CPU), and the y-axis indicates the average access latency per cacheline in nanoseconds. Each test accesses more than 32GiB of memory and repeats 1000 times to obtain average latency values.

better optimized CXL memory controller that can efficiently reduce the access latency, compared to AMD-Zen4’s controller.

In addition, we observe that Intel-SPR’s multi-NUMA link behaves differently from AMD-Zen4’s. This is from our observation that on Intel-SPR, CXL access overhead is more consistent in local and remote accesses, while AMD-Zen4’s access latency overhead is less uniform: On Intel-SPR, the ASIC-CXL has a $1.94\times$ higher latency over DRAM under sequential local access, and it’s $1.76\times$ on sequential remote access. While on AMD-Zen4, it’s $2.12\times$ and $1.68\times$, respectively, presenting a larger variance than Intel-SPR. The same trend applies to random access, where Intel-SPR’s CXL has $1.92\times$ and $1.75\times$ higher latency on local and remote accesses, while AMD-Zen4’s CXL expander has $2.06\times$ and $1.66\times$. We observe the main reason behind this discrepancy is that AMD-Zen4’s multi-NUMA link introduces more latency than Intel-SPR’s.

Store Latency: A similar trend with the load latency is observed in the store latency results (Figure 2b): The FPGA-CXL and ASIC-CXL’s store latency is always higher than that of DIMM. With Intel-SPR, ASIC-CXL is $1.71\times$ slower than DRAM when the benchmark sequentially accesses local nodes and is $1.67\times$ slower in the sequential remote. While with AMD-Zen4, ASIC-CXL’s overhead is not uniform, reaching $2.1\times$ for sequential local access and $1.69\times$ for sequential remote ones. Remote access also exhibits such discrepancies between Intel-SPR and AMD-Zen4 CPUs.

Overall, these observations confirm that the baseline load/store latency of CXL memory is higher than that of DIMM, with further variations depending on the CPU vendor.

Observation 1. Intel-SPR’s CXL memory expander consistently demonstrates not only better latency performance than AMD-Zen4’s CXL memory expander but also maintains a uniform load/store latency difference between remote and local access relative to DIMM. In contrast, AMD-Zen4 shows a notable discrepancy in load/store latency between local and remote access.

3.2 Bandwidth Scaling

We configured HEIMDALL to measure the bandwidth of different NUMA nodes with different numbers of CPU threads. As shown in Figure 3, the bandwidth scaling depends on the CXL device type and the CPU vendor. “Local” refers to the performance when the memory device is connected to the same NUMA node as the CPU cores running the profiling, while “Remote” refers to the performance when the memory is on a different socket. For DIMM, we measured the values of the local node (NUMA 0) and remote node (NUMA 1) from socket 0. To test the CXL memory node (NUMA 2) connected to the PCIe slot of socket 0, we used the cores of socket 0 for the local tests and the cores of socket 2 for the remote tests. To measure the maximum bandwidth, we enabled Hyper-threading during the test.

FPGA-CXL vs. ASIC-CXL. In this section, we compare the bandwidth scaling results for FPGA-CXL and ASIC-CXL on load and store access, respectively. We begin with the load access comparison. By examining the performance of

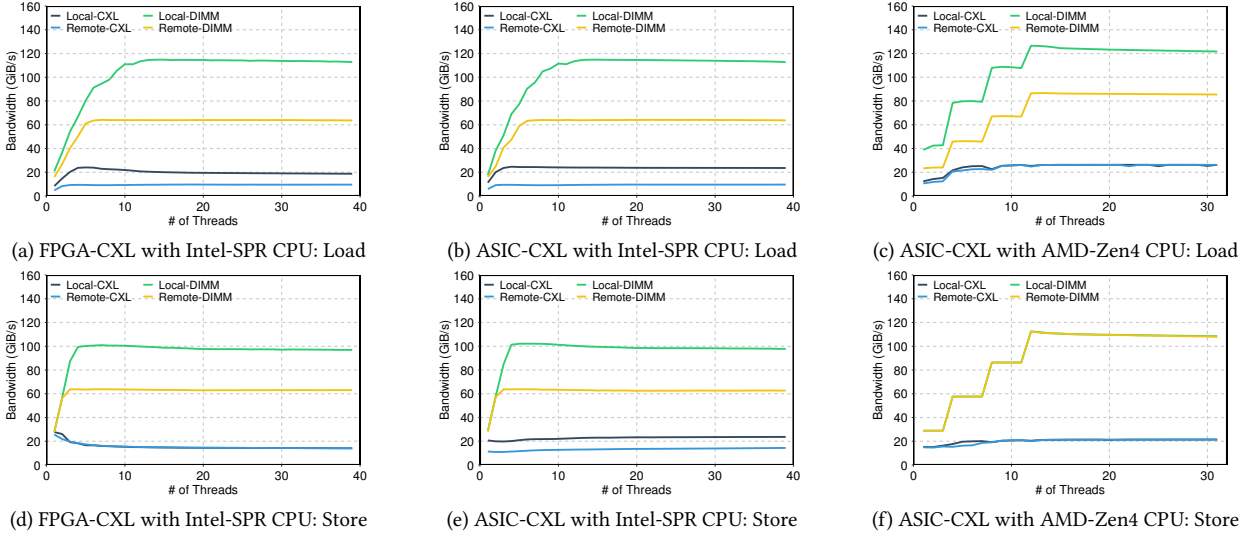


Figure 3: Bandwidth scaling when using different number of threads. The x-axis is the number of threads accessing memory, and the y-axis is the peak bandwidth achieved. We measure memory bandwidth accessing from both local and remote CPUs.

FPGA-CXL and ASIC-CXL on the same Intel-SPR platform (Figure 3a and Figure 3b), we find that ASIC-CXL provides better support for concurrent access: When using a small number of threads, both FPGA-CXL and ASIC-CXL achieve a similar bandwidth scaling. Once threads increase over four, FPGA-CXL bandwidth drops for local accesses, while ASIC-CXL remains stable. The FPGA-CXL has only two SODIMMs (Table 1) as its device memory, and this limited number of channels may cause worse scaling compared to ASIC-CXL’s implementation where many DDR5 modules are directly soldered on board.

For store operations, FPGA-CXL shows worse performance than ASIC-CXL. As thread count increases, the bandwidth of FPGA-CXL decreases and eventually levels off, reaching similar saturation on both remote and local access, with peak performance achieved only at a single thread. In contrast, ASIC-CXL consistently maintains saturated bandwidth with minimal variation as thread count increases, and the bandwidth difference between local and remote access remains steady. Compared to load access, neither expanders show effective bandwidth scaling of store access on Intel-SPR.

AMD-Zen4 CPU Figure 3c shows the bandwidth vs. thread performance for the load access on the AMD-Zen4 CPU server. Two key observations can be made from this data. First, the bandwidth increase for DIMM follows a stepwise pattern, unlike the smoother increase seen with the Intel-SPR CPU (as shown in Figure 3b). This step pattern aligns with the AMD Genoa architecture’s Core Complex (CCX), where each unit consists of four cores that share the last-level cache. After 12 threads, both local and remote DIMM bandwidth saturate, reaching 122 GiB/s and 85 GiB/s, respectively. The second observation is that both local and remote CXL memory bandwidth saturates at similar values, around 26 GiB/s, with nine threads being the point of saturation for both.

Figure 3f presents the bandwidth versus thread performance for store access, with two notable observations. First, the bandwidth increase for DIMM also follows a stepwise pattern similar to load access; however, unlike the load case, local and remote bandwidth exhibit similar increases, causing the lines to overlap. Each step corresponds to four threads, matching the CCX size of the AMD Genoa architecture. After 12 threads, both local and remote bandwidth saturate at the same level of 116 GiB/s. The second observation is that local and remote CXL memory bandwidth saturates at similar values, approximately 20 GiB/s.

Intel-SPR CPU Figure 3b illustrates the bandwidth vs. thread profiling for the load access on the Intel-SPR CPU server. There are two notable differences compared to the AMD-Zen4 results. First, the bandwidth increase for DIMM in the Intel-SPR CPU shows a smooth, continuous curve, unlike the stepwise pattern observed in AMD-Zen4. The local DIMM bandwidth saturates at 114 GiB/s with nine threads, while the remote DIMM bandwidth reaches saturation

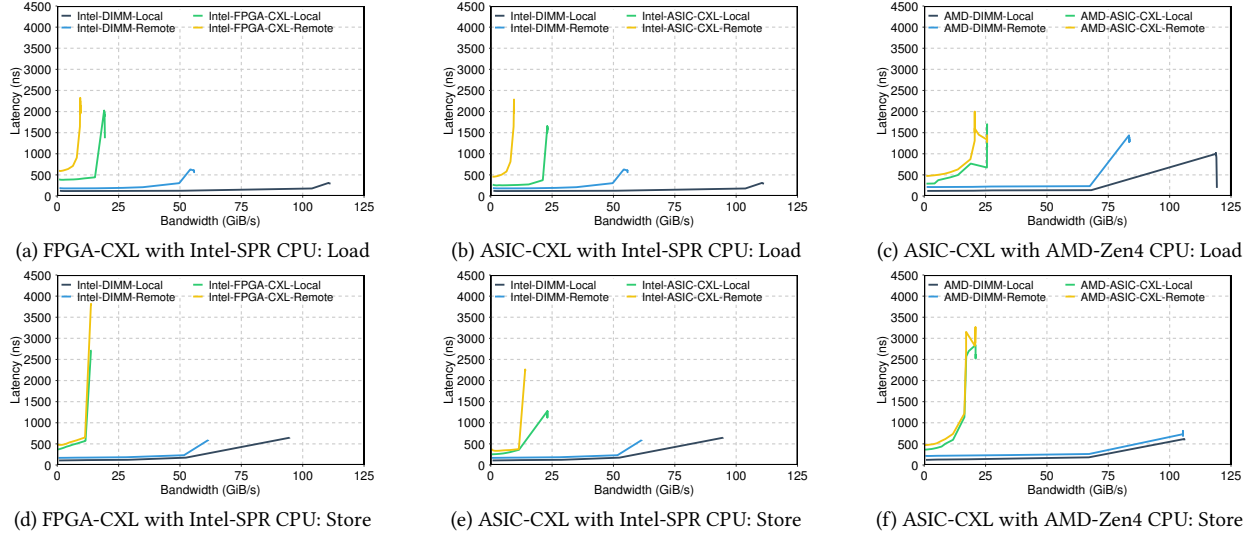


Figure 4: Bandwidth vs. latency measurements on each machine, where we measure from both local and remote CPUs, accessing either DRAM DIMM or the CXL memory.

at 63 GiB/s with six threads. The second difference is that, unlike AMD-Zen4, the remote and local CXL memory bandwidths on Intel-SPR are saturated at different levels. Local CXL bandwidth reaches 23 GiB/s with three threads, while remote CXL bandwidth is limited to 9 GiB/s, saturating with just two threads.

Figure 3e shows the bandwidth versus thread profiling for store access on the Intel-SPR CPU server, with two key observations. First, the bandwidth scaling curve is smoother than that of AMD-Zen4. The local DIMM bandwidth saturates at nearly 102 GiB/s with four threads, while remote DIMM reaches saturation at 63 GiB/s with three threads. Second, Intel-SPR shows a consistent bandwidth gap between remote and local CXL memory, with local bandwidth at 23 GiB/s and remote at 13 GiB/s, maintaining an approximate 10 GiB/s difference. Compared to DIMM, the ASIC-CXL does not support bandwidth scaling effectively on Intel-SPR.

Observation 2. ASIC-CXL shows more stable bandwidth scaling compared to FPGA-CXL. In addition, CXL memory on AMD-Zen4 shows better bandwidth performance than CXL memory on Intel-SPR, with similar saturation levels for local and remote access, while Intel-SPR’s CXL memory saturates at different bandwidth between local and remote access.

3.3 Bandwidth vs. Latency

In this section, we profile the changes in latency as the bandwidth increases for CXL memory and DIMM memory to identify the latency characteristics of CXL memory compared to DIMM based on bandwidth. Additionally, we seek to determine the optimal bandwidth level for using CXL memory that expands system bandwidth without degrading system performance. Figure 4 presents our bandwidth vs. latency measurements for CXL and DIMM devices on both AMD-Zen4 and Intel-SPR CPU servers, comparing local and remote performance. The x-axis represents bandwidth, and the y-axis shows latency.

Intel-SPR CPU Figure 4a and Figure 4b illustrate the bandwidth vs. latency performance for the Intel-SPR CPU server, comparing CXL memory and DIMM in both local and remote configurations. The CXL memory expander on the Intel-SPR system, using PCIe 5.0 with 8 lanes (32 GT/s per lane), achieves 74% of the theoretical maximum bandwidth of 32 GiB/s with a latency of 1.65 μ s for local memory, and 30% with 1.99 μ s for remote memory. The Intel-SPR system’s four DDR5 DIMM modules (32 GiB each) connected at 4800 MT/s achieve a theoretical maximum of 150 GiB/s per NUMA node. Local DIMM achieves 65% of this bandwidth, while remote DIMM reaches 38%, yielding a local-to-remote bandwidth difference of 1.99 \times . Comparing local DIMM to local CXL, the DIMM achieves 4.83 \times higher bandwidth and 2.14 \times lower latency. For remote memory, DIMM exhibits 5.87 \times higher bandwidth and 2.54 \times

lower latency than CXL.

Figure 4e shows the bandwidth versus latency performance for store operations on the Intel-SPR CPU server, with two key observations. First, local CXL memory achieves 74% of the theoretical maximum bandwidth of 32 GiB/s, with a latency of 1.28 μ s, while remote CXL memory achieves 45% of the theoretical bandwidth with a latency of 2.27 μ s, resulting in 1.78 \times higher latency for remote memory. Second, the performance comparison of CXL memory expanders and DIMMs reveals that the Intel-SPR CPU, equipped with four 32 GiB DIMM modules per NUMA node at 4800MT/s, achieves a theoretical maximum bandwidth of 150 GiB/s per NUMA node. Local DIMM achieves 64% of this bandwidth, while remote DIMM achieves 42%, with a local-to-remote bandwidth difference of 1.54 \times . When comparing local DIMM and local CXL, DIMM provides 3.85 \times higher bandwidth and 1.97 \times lower latency. For remote memory, DIMM offers 4.22 \times higher bandwidth and 3.82 \times lower latency than CXL.

AMD-Zen4 CPU Figure 4c presents the bandwidth vs. latency performance of load operations on the AMD-Zen4 CPU server, highlighting two key observations. First, the comparison between local and remote CXL memory shows that both achieve 82% of the theoretical maximum bandwidth of 32 GiB/s, based on PCIe 5.0 (8 lanes), with latencies of 1.15 μ s and 1.45 μ s, respectively. The remote memory exhibits 1.28 \times higher latency than local memory, though the bandwidth remains identical. Second, the analysis compares the performance of CXL memory expanders and DIMMs. The AMD-Zen4 CPU, equipped with four 16 GiB DIMM modules per NUMA node at 4800 MT/s, achieves a theoretical maximum bandwidth of 150 GiB/s per NUMA node. Local DIMM achieves 81% of this bandwidth, while remote DIMM achieves 57%, resulting in a local-to-remote bandwidth difference of 1.43 \times . When comparing local DIMM and local CXL, the DIMM demonstrates 4.65 \times higher bandwidth and 3.94 \times lower latency. Similarly, for remote memory, DIMM shows 3.26 \times higher bandwidth and 1.38 \times lower latency than CXL.

Figure 4f illustrates the bandwidth versus latency performance for store operations on the AMD-Zen4 CPU server, with two notable insights. First, local and remote CXL memory reach 67% of the theoretical maximum bandwidth of 32 GiB/s, with latencies of 2.85 μ s and 3.28 μ s, respectively. Remote memory exhibits 1.14 \times higher latency than local memory. Second, comparing CXL memory expanders and DIMMs shows that the AMD-Zen4 CPU, equipped with four 16 GiB DIMM modules per NUMA node at 4800MT/s, achieves a theoretical maximum bandwidth of 150 GiB/s per NUMA node, with both local and remote DIMMs reaching 72% of this capacity. Comparing local DIMM and local CXL, DIMM shows 5.07 \times higher bandwidth and 5.60 \times lower latency. For remote memory, DIMM exhibits 5.04 \times higher bandwidth and 4.02 \times lower latency than CXL.

When comparing the AMD-Zen4 and Intel-SPR CPU servers, for the load access, AMD-Zen4’s local CXL memory expander exhibits 1.89 \times higher latency but 1.11 \times better bandwidth than Intel-SPR’s CXL memory expander. For remote CXL memory, AMD-Zen4 demonstrates 2.69 \times better bandwidth, although with 1.04 \times higher latency than Intel-SPR. On the remote access, Intel-SPR’s local CXL memory expander exhibits 2.3 \times lower latency and 1.10 \times higher bandwidth than AMD-Zen4’s CXL memory expander. For remote CXL memory, AMD-Zen4 demonstrates 1.49 \times better bandwidth, although with 1.44 \times higher latency than Intel-SPR.

Observation 3. ASIC-CXL shows higher bandwidth performance with lower latency compared to FPGA-CXL CXL. When comparing AMD-Zen4 and Intel-SPR CXL, AMD-Zen4 CXL achieves higher bandwidth performance, while Intel-SPR CXL shows an advantage in latency.

3.4 Bandwidth of NUMA Interleaving

In this section, we explore methods to extend memory bandwidth using a CXL memory expander, with a focus on maximizing bandwidth through heterogeneous memory interleaving. We first introduce basic approaches to attaching CXL memory for bandwidth enhancement, followed by methods for managing heterogeneous memory interleaving. Finally, we present profiling results for the introduced interleaving methods, highlighting the impact of varying interleaving weights between DIMM and CXL memory.

3.4.1 Memory Bandwidth Expansion with CXL

By integrating a CXL memory expander, we can increase both memory capacity and bandwidth, as it enables the use of CXL bandwidth in addition to traditional DIMM bandwidth. To enhance bandwidth and capacity with a CXL memory expander, two fundamental approaches are available.

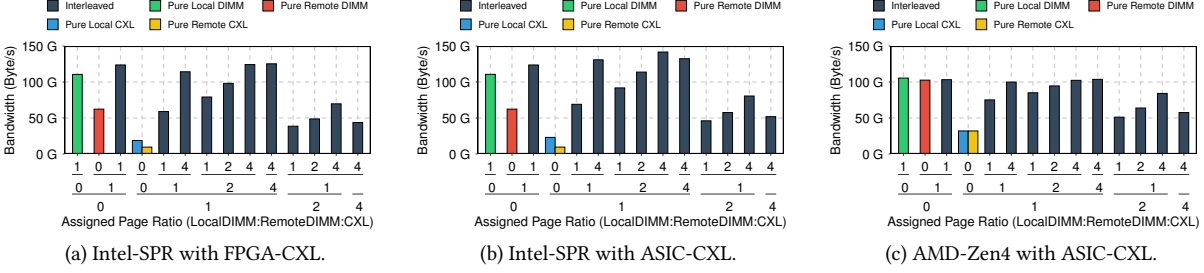


Figure 5: Bandwidth vs Weighted NUMA interleave

CXL Direct-Attached Memory Tiering: In this approach, the CXL memory expander is attached directly to the root complex without network devices like switches or fabrics to maximize bandwidth and capacity. This method is especially beneficial for applications constrained by bandwidth or latency. However, it is limited by the number of available CXL flex slots, restricting the number of directly attached devices. This approach has been available since the CXL1.0 specification, which supports direct attachment.

CXL Switches and Fabric-Attached Memory Tiering: CXL memory modules are connected through fabric and switch networks, allowing for greater bandwidth and capacity expansion but with added latency. Although this approach offers higher scalability than direct attachment, it requires a compromise due to the additional latency introduced by the fabric and switch components. This method is subject to CXL specification limitations. Single-level switch memory tiering requires devices that support the CXL2.0 specification, while multi-level switch and fabric topology require CXL3.0-compliant devices.

3.4.2 Heterogeneous Memory Interleaving with CXL

After attaching the CXL memory expander to the system using one of the methods described in Section 3.4.1, implementing efficient memory management policies becomes essential to maximize overall memory bandwidth. There are three foundational methods to interleave memory and we present our profiling results of the software-based approach.

Hardware-Based Heterogeneous Interleaving: This method involves configuring the system address map in the BIOS to interleave between DIMM and CXL memory expanders. However, this approach has limitations; the OS or kernel cannot control memory allocation in interleaved configurations, and applications that do not benefit from interleaving may experience inefficiencies due to the lack of control.

Hardware + Software Based Heterogeneous Interleaving: In this method, hardware assigns DIMM channels to different NUMA nodes, while software tools such as numactl set the interleaving ratio between DIMM and CXL memory. This approach allows the OS or kernel to manage memory allocation more effectively, but it lacks flexibility for dynamic workloads because its interleaving ratio is pre-defined instead of being dynamically adjusted at runtime.

Software-Based Heterogeneous Interleaving: This method enables memory allocation by configuring weights for each NUMA node at the application level. Based on these assigned weights, the kernel manages page allocation during interleaving. For example, consider a system with three NUMA nodes: NUMA0 and NUMA1 connected to DIMM, and NUMA2 connected to a CXL memory expander. The application sets weights for each NUMA node—2, 2, and 1, respectively—in the Linux kernel at `/sys/kernel/mm/mempolicy/weighted-interleave/node-number`. When the application interleaves 100 pages, the kernel allocates 40 pages each to NUMA0 and NUMA1, and 20 pages to NUMA2. This approach allows for flexible adjustment of interleaving weights, enabling optimized memory performance tailored to specific applications and workload characteristics.

3.4.3 Weighted NUMA Interleaving Results of the Heterogeneous Memory

For profiling the bandwidth of heterogeneous memory interleaving, we used the CXL Direct-Attached Memory Tiering approach in combination with Software-Based Heterogeneous Interleaving. We checked the weighted interleaving behavior on AMD-Zen4 and Intel-SPR with ASIC-CXL and FPGA-CXL based on the same system setup. Figure 5

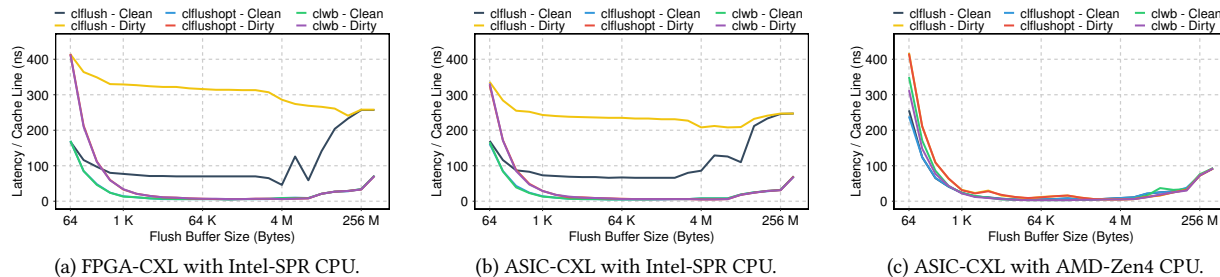


Figure 6: Flush latency when flushing different sized data, all results are from local accesses with pointer-chasing random access pattern. We measured flushing either modified cachelines (“Dirty”) or the unmodified cachelines (“Clean”). The `clwb` has similar latency to `cflushopt` on Intel-SPR CPU, thus their corresponding lines are overlapping in Intel-SPR figures.

presents the weighted interleaving result. x-axis represents the weighted interleaving ratios between local DIMM (NUMA0), remote DIMM (NUMA1), and CXL memory (NUMA2). The y-axis shows the bandwidth value.

FPGA-CXL vs ASIC-CXL. Figure 5a and Figure 5b show the weighted interleaving results for FPGA-CXL and ASIC-CXL, respectively. Comparing the interleaving results reveals that ASIC-CXL consistently achieves higher bandwidth than FPGA-CXL, with an average difference of 8.40 GiB/s, a maximum difference of 17.46 GiB/s, and a minimum difference of 0.04 GiB/s.

The FPGA-CXL demonstrates limited impact on memory bandwidth improvement; for instance, in the weighted interleaving configuration with DIMMs only (1:1:0), the bandwidth reaches 123.67 GiB/s, whereas the 4:4:1 configuration yields only a slight increase to 125.26 GiB/s. This suggests that the FPGA-CXL offers a minimal contribution to memory bandwidth expansion. In contrast, the ASIC-CXL exhibits significantly better bandwidth enhancement capabilities than FPGA-CXL. In the DIMMs only (1:1:0) configuration, Intel-SPR with ASIC-CXL achieves 123.63 GiB/s, increasing to 141.64 GiB/s in the 4:2:1 configuration. This suggests that ASIC-CXL provides better support for weighted NUMA interleaving than FPGA-CXL.

Observation 4. ASIC-CXL demonstrates better bandwidth scalability with weighted NUMA interleaving compared to FPGA-CXL, achieving higher bandwidth gains across configurations.

AMD-Zen4 vs Intel-SPR with ASIC-CXL Figure 5b and Figure 5c present the weighted interleaving results for Intel-SPR and AMD-Zen4 with ASIC-CXL. The results indicate that AMD-Zen4 does not effectively support the weighted interleaving method. For example, when comparing the results of pure local DIMM, pure remote DIMM, and the 1:1:0 configuration, the 1:1:0 configuration shows similar bandwidth performance despite simultaneous usage of remote and local DIMMs. In contrast, Intel-SPR demonstrates better bandwidth scaling when the CXL memory expander is added. The maximum bandwidth difference between Intel-SPR and AMD-Zen4 is observed at 39.02 GiB/s in the 4:2:1 configuration. This suggests that Intel-SPR achieves superior bandwidth scaling with weighted NUMA interleaving compared to AMD-Zen4.

Observation 5. Intel-SPR achieves superior bandwidth scaling with weighted NUMA interleaving compared to AMD-Zen4, especially when the CXL memory expander is added.

3.5 Flush Instructions

In this section, we evaluate how the CXL memory expander supports flush instructions by testing the latency of various flush operations (`cflush`, `cflushopt`, `clwb`) under different conditions on both AMD-Zen4 and Intel-SPR CPUs. The `cflush` instruction flushes all data in a cache line to memory and invalidates the cache line. Similarly, `cflushopt` flushes the cache line data to memory and invalidates it, but unlike `cflush`, it can flush multiple cache lines simultaneously within the same thread, making it more efficient for flushing large buffers (e.g., larger than

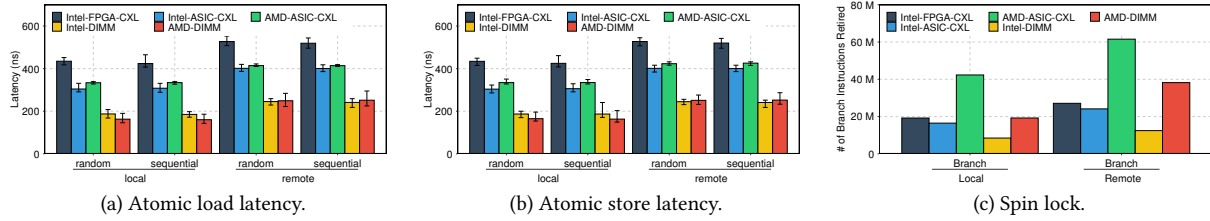


Figure 7: Atomic operations on CXL are slower and causes more branch instructions to be executed.

several KiB). The `c1wb` instruction, like `c1flushopt` and `c1flush`, flushes the cache, but instead of invalidating the cache line, it writes back dirty data to memory and keeps the cache line valid, thus improving performance by increasing the cache hit ratio [15].

For this test, we used an in-house micro-benchmark framework capable of measuring the latency of the three flush instructions. This framework can support both modified and unmodified cache states. The unmodified cache state refers to data that has not been changed by store operations, meaning the cache line is clean. In contrast, the modified state refers to cache lines where the data has been rewritten, resulting in dirty cache lines. Additionally, the benchmark allows adjustment of the flush buffer size, ranging from 64 B to the LLC buffer size of each CPU core, to test performance across different buffer sizes.

Figure 6 shows the latency test results according to flush buffer size on Intel-SPR and AMD-Zen4 CPUs, respectively. The x-axis represents the flush buffer size in bytes, and the y-axis shows the latency per cache line in nanoseconds. These two graphs illustrate how the latency for cache line flushing changes as the flush buffer size increases.

Intel-SPR CPU From Figure 6a and Figure 6b, we find that both `c1flushopt` and `c1wb` show improved performance as the flush buffer size increases. This is because these instructions can flush multiple cache lines simultaneously within the same thread, allowing the number of cache lines being flushed in parallel to increase with buffer size, leading to better performance. In modified cache scenarios, both `c1wb` and `c1flushopt` outperform `c1flush` by up to $76.33\times$. In unmodified cache scenarios, `c1wb` shows a performance increase of up to $33\times$ compared to `c1flush`, while `c1flushopt` improves by up to $22\times$.

Observation 6. When flushing multiple cache lines simultaneously, `c1wb` generally provides the best latency, followed by `c1flushopt` and `c1flush`.

AMD-Zen4 CPU From Figure 6c, the key observation for AMD-Zen4 CPUs shows a different trend from Intel-SPR CPUs. As the buffer size increases, the latency for all three flush instructions converges beyond 4 KiB. Interestingly, for flush buffer sizes smaller than 4 KiB, `c1wb`, which generally outperforms `c1flush` on Intel-SPR CPUs, shows the worst performance in unmodified cache states on AMD-Zen4 CPUs, with latency being $1.49\times$ worse than `c1flush`. However, in modified cache scenarios, `c1wb` performs the best, providing a $1.43\times$ improvement over `c1flush`.

Observation 7. When flushing data smaller than 4 KiB, `c1wb` and `c1flushopt` provide lower latency. This effect is more obvious on Intel-SPR than AMD-Zen4 CPUs.

3.6 Atomic Instructions

In this section, we explore how the atomic instructions work with CXL system. Atomic instructions play a critical role in multi-core, multi-threaded computing environments. They guarantee that a single operation is executed without interruption, preventing other instructions from accessing the affected memory until the operation is completed. This is crucial for implementing synchronization primitives like locks, semaphores, and other concurrency control mechanisms.

With the introduction of CXL, the memory ecosystem has expanded. Since CXL.io is based on PCIe and PCIe starts to support atomic operations from 3.0, we conduct experiments to verify whether atomic instructions are effectively

supported on shared memory resources using CXL memory expanders. The results confirm that CXL memory has supported all the x86 atomic operations, including `CMPXCHG` and other instructions that support the `LOCK` prefix. We also measure the atomic load and store latency of CXL memory using `CMPXCHG` instructions, with all hardware prefetchers disabled during testing. The results are presented in Figure 7(a) and Figure 7(b). The latency is similar to the regular load and store latency shown in Figure 2.

When the operation is not supported in a native x86 atomic instruction, methods such as spinlock or mutex are needed to maintain synchronization. We study the potential spinlock overhead caused by CXL memory. In this test, two threads share data. Each thread writes a random value to the shared data and then executes a flush operation on it. To maintain synchronization, a spinlock is applied before the write and released after the flush. We measure the number of executed branches in the spinlock loop using the `perf` tool. As shown in Figure 7(c), when the data is allocated in CXL memory, there is a significantly higher branch count, indicating that the CPU spends more time spinning and waiting for the lock. This increase is due to the higher latency of CXL memory, which increases the execution time for each thread and, consequently, causes threads to spend more time in the busy-looping state while waiting for the lock. On AMD-Zen4, the spinlock overhead for both DIMM and CXL memory is more than 100% higher than on Intel-SPR, exceeding their memory latency difference, suggesting that Intel-SPR may have better optimizations to reduce CPU spinning. In summary, when running workloads with frequent spinlock operations on CXL memory, CPU spinning becomes a significant issue, and strategies like increasing the sleep time within the spinlock loop can be considered to help mitigate this overhead.

4 Micro-Architecture Characteristics

4.1 CPU Cache Utilization of CXL Memory

This section provides an in-depth analysis of CPU cache utilization for CXL memory. The discussion and figures primarily focus on the configuration of Intel-SPR with ASIC-CXL. Any differences observed in the configurations of Intel-SPR with FPGA-CXL and AMD-Zen4 with ASIC-CXL will be specifically noted.

4.1.1 Basic Utilization

Previous studies have revealed that PCIe peripherals, such as NICs, can utilize only a limited portion of the CPU’s Last-Level Cache (LLC) through Direct Data I/O (DDIO) [16, 17]. Given that the `CXL.io` protocol is also built on PCIe, we aim to investigate the cache utilization characteristics of CXL memory devices.

Our experiments evaluate cache utilization in both local and remote CXL access scenarios. We also test different types of load/store instructions, including regular, non-temporal, and atomic operations.

Regular Load/Store: Figure 8b and Figure 8e show heat maps of CXL load latency on Intel-SPR with ASIC-CXL. The deep blue areas represent low latency, meaning the pointer-chasing data fits well within the CPU cache. Outside of these blue areas, latency increases due to cache evictions. By looking at the edges of the blue region, we can estimate the size and associativity of the CPU cache.

In Figure 8b, where data comes from a local CXL device, the entire LLC is used. In contrast, Figure 8e shows that remote CXL access only uses a small part of the LLC, with a smaller low-latency area. The maximum size of this area is 4 MiB, which is about 1/8th of the total LLC size. Similar results are observed for store operations, and the results are consistent across different CXL memory devices.

The asymmetry persists on FPGA-CXL (Figure 8a and Figure 8d). We perform the same tests on DIMM DRAM. Both local and remote DIMM access fully utilize the LLC size. This suggests that the issue with Intel-SPR might be due to its implementation of the CXL controller on the CPU side. We also test the CXL device on AMD-Zen4. The results (Figure 8c and Figure 8f) show that the local and remote CXL accesses have symmetric LLC utilization. Therefore, programmers should be careful when using remote CXL on Intel CPUs in data-intensive and latency-sensitive tasks, as limited cache use may lead to higher average latency.

Non-Temporal Load/Store: We also test non-temporal operations, which are designed to bypass the cache for data that is unlikely to be reused soon, aiming to reduce cache pollution. On Intel-SPR, we observe that non-temporal

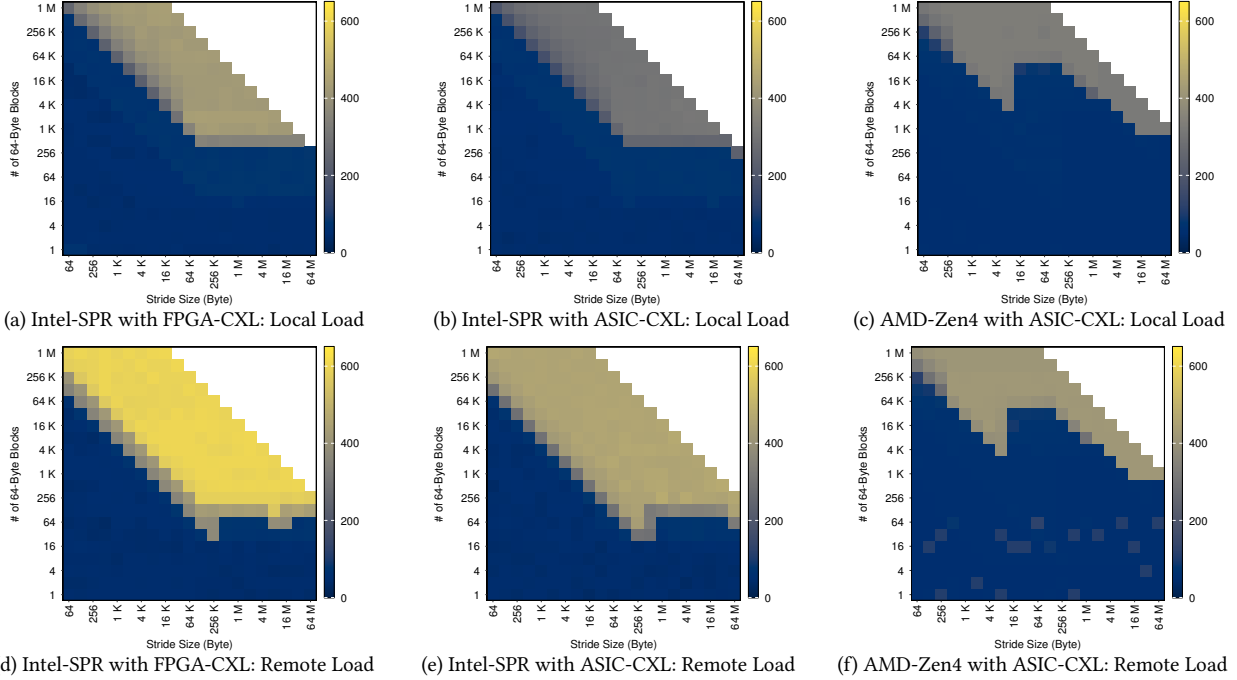


Figure 8: Cache utilization of local and remote CXL read in different systems.

loads, whether from DIMM or CXL, still utilize the LLC cache, similar to regular loads. The asymmetry between local and remote CXL still exists. In contrast, on AMD-Zen4, non-temporal loads bypass the LLC and instead use caches in higher levels. For non-temporal stores, regardless of whether on Intel-SPR or AMD-Zen4, and whether using DIMM or CXL memory, cache usage is always bypassed.

Atomic Load/Store: Section 3.6 demonstrates that the CXL device supports all x86 atomic instructions. We also evaluate the cache utilization of atomic operations, and the results are consistent with those observed for regular load/store operations.

Observation 8. On Intel-SPR, remote CXL access cannot fully utilize LLC. The maximum LLC size available for it is limited to 4 MiB on our test machines with 38 MiB LLC. This limitation is unrelated to the CXL device implementation and types of memory operations.

4.1.2 Under SNC Mode

In SNC (Sub-NUMA Clustering) mode, the CPU divides a single chip into multiple NUMA nodes, each managing its portion of the LLC. Our Intel-SPR machine supports up to SNC2, which splits the chip into two NUMA nodes, and each node controls half of the LLC. When running the pointer-chasing task on one node, if the data comes from local DIMM DRAM, only half of the LLC is utilized, following the SNC partitioning, shown in Figure 9a. However, remote socket DIMM access (Figure 9b) can still use the entire size of the LLC.

For CXL memory devices, it is observed that even with local CXL, the entire LLC size is used, as Figure 9c shows. This result is consistent with the previous finding [18]. This indicates that SNC does not enforce strict LLC partitioning under both remote DIMM and local CXL accesses. For remote CXL (Figure 9d), the LLC usage remains limited to 4MB, and it is shared across two NUMA nodes on the same socket. AMD has a similar feature called Nodes per Socket (NPS). However, on AMD-Zen4, we do not observe LLC partitioning on either DIMM DRAM or CXL, as Figure 10 shows.

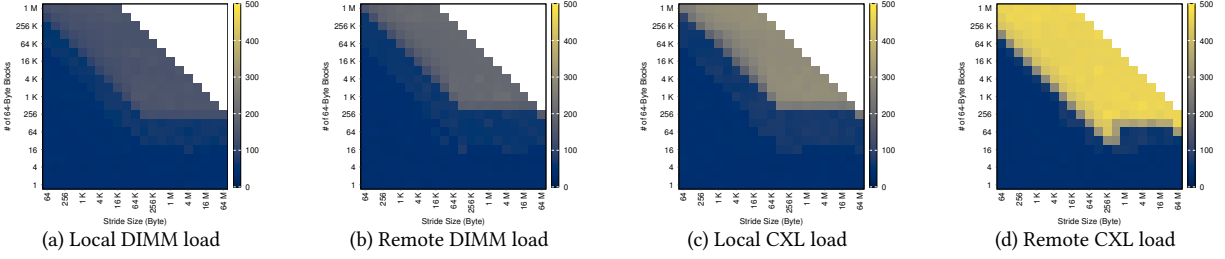


Figure 9: Cache utilization under SNC2 on Intel-SPR with ASIC-CXL

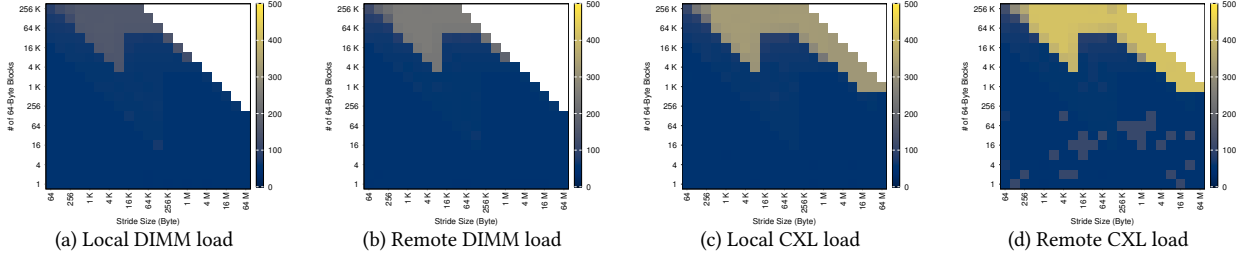


Figure 10: Cache utilization under NPS2 on AMD-Zen4 with ASIC-CXL

4.1.3 Under Intel CAT

Intel CAT (Cache Allocation Technology) [19] is another method for cache partitioning. CAT allows the creation of multiple Classes of Service (CLOS), each associated with a mask. The bits set to 1 in this mask represent the cache ways or slices that the corresponding CLOS can utilize. By binding a CLOS to specific processes or CPU cores, cache partitioning can be effectively implemented. Intel-SPR support both L2 and LLC CAT.

We test whether CXL memory follows CAT partitioning. The result is shown in Figure 11. For example, when the LLC CAT mask is set to 0xff (the default is 0x7fff), we observe that the LLC size available to CXL memory is reduced, allowing only about half of the associativity to be used. We test various masks and confirm that both local and remote CXL memory data follow CAT-based cache partitioning. L2 CAT also works on CXL memory.

Observation 9. On Intel-SPR, data from CXL memory and remote DIMM memory do not follow the LLC partitioning under Sub-NUMA Clustering (SNC) mode. For strict global LLC partitioning requirements, Intel Cache Allocation Technology (CAT) is recommended.

4.1.4 Remote CXL Access

This section provides an in-depth study of remote CXL access on a dual-socket NUMA system (Intel-SPR), focusing on both the cache allocation policy and the data path analysis.

Cache Allocation Policy: The DDIO cache typically utilizes a fixed LLC location [16]. Given that remote CXL access also uses a limited LLC capacity, we investigate whether it follows a similar caching mechanism. First, we test the remote CXL access cache utilization with DDIO function disabled. The results still show that it has a limited LLC usable size. Then we investigate where this region is located in the LLC. In the experiment, there are two processes: P0 and P1. P0 accesses data from remote CXL, while P1 accesses data from local DIMM. Both processes run on separate physical cores, each bound a specific CAT mask.

From previous CAT tests, a mask with four consecutive ‘1’ bits restricts the cache size to the same amount as the upper limit of remote CXL data’s usable LLC size. First, we run P0 with a 4-bit ‘1’ CAT mask and change the mask locations to see if the remote CXL LLC region can be changed by CAT. P1 also uses a 4-bit ‘1’ CAT mask. During each test, we keep P0’s mask fixed and shift P1’s mask to observe where LLC eviction occurs. The results are shown in Figure 12a. We measure the average access latency of P1. For each P0’s mask, the latency spike of P1 consistently

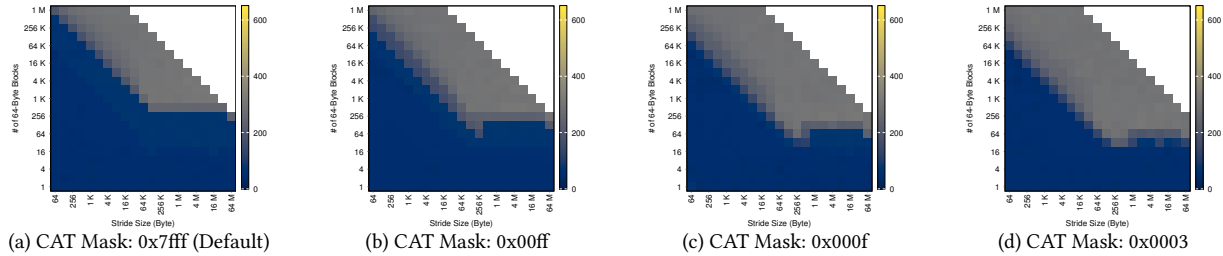


Figure 11: Cache utilization of local CXL load under different CAT masks on Intel-SPR with ASIC-CXL

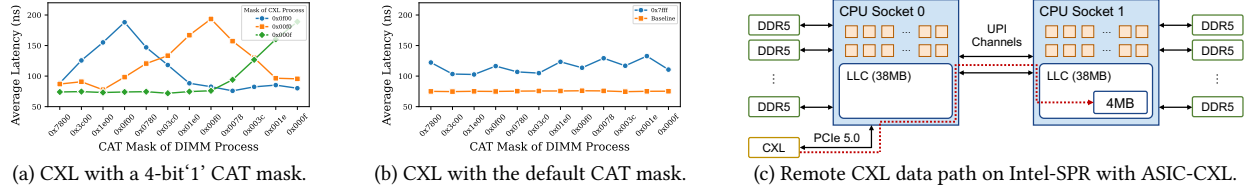


Figure 12: (a) (b) Remote CXL access with different CAT masks on Intel-SPR with ASIC-CXL. (c) CXL data path when accessing from remote CPU socket.

appears under the exact same CAT mask with P0, suggesting that both processes share the same LLC region and cause eviction with each other. This implies that the LLC region utilized by remote CXL data can be altered by modifying the CAT mask.

Next, we investigate whether remote CXL access has a preferred LLC region under the default CAT mask (0x7fff on Intel-SPR). The "Baseline" in Figure 12b represents the scenario where only P1 is running, resulting in all data hitting the LLC. When both P0 and P1 are running, if P0 is using a fixed cache region, we will expect a latency spike similar to Figure 12a. However, no such spike is observed during the test. While the average latency remains significantly higher than typical LLC hit latency, indicating that eviction is occurring, this suggests that remote CXL data may dynamically select its limited-size LLC region, different from DDIO cache.

Observation 10. On Intel-SPR, the limited LLC region location for remote CXL data can be dynamically altered, different from DDIO cache policy.

Data Path Analysis: Next, we analyze the data path of remote CXL access. To determine whether remote CXL data traverse the Intel Ultra Path Interconnect (UPI) or only the PCIe root complex to reach the destination socket, we conduct a bandwidth test for remote CXL access while simultaneously monitoring UPI activity using Intel PCM [14]. During the bandwidth test, the UPI occupancy rate reaches 20% to 30%, indicating that remote CXL access utilizes UPI as its data path.

In addition, we analyze the cache footprint of remote CXL access. When a socket directly accesses remote CXL data, the data only stays in the destination socket’s LLC rather than both sockets’. Figure 12c shows the data path of directly accessing CXL data from the remote socket.

We further explore if first placing the data in the local socket’s LLC and then reading it from the remote socket could bypass the LLC size limitation for remote CXL data. First, we allocate a shared data block that is larger than 4 MB but smaller than the LLC size. Then, we run thread 0 on the local socket, randomly accessing all the shared data and recording the average access time. After multiple iterations, since all the data is stored in the cache, the average access time is below 50 ns, and the cache miss rate is low. Next, we run thread 1 on the remote socket, similarly accessing all the shared data repeatedly. The results show that when the shared data comes from DIMM DRAM (regardless of which socket it belongs to), the average access latency for thread 1 is similar to thread 0, and the cache miss rate remains low. This is because the shared data eventually gets cached in the remote socket’s LLC. However, when the data comes from CXL memory, thread 1’s average access latency increases to 100–150 ns, and the cache miss rate

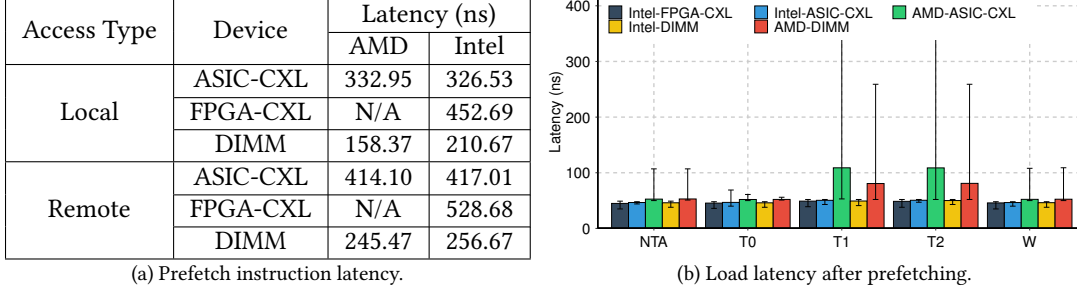


Figure 13: Prefetching measurements: Figure 13a shows the latency of executing the T0 prefetch instruction on different systems, and Figure 13b presents the load latency after issuing different types of prefetch instructions.

increases significantly. This is due to the remote socket being unable to store all the data in its LLC, causing some data to be evicted back to the local socket’s cache.

This indicates that even when CXL data is already stored in the local socket’s LLC, accessing this data from the remote socket still faces the LLC size limitation. Therefore, we can confirm that as long as the data originates from CXL memory, the LLC size limitation persists on the remote socket. We assume that this may be due to the CPU identifying the data as originating from a remote node via the physical address during the address translation process, thereby adopting a different cache mechanism.

Observation 11. When the remote socket directly accesses CXL data, the data are cached only in the remote socket, not both. Caching CXL data in the local socket first and then moving it to the remote socket does not bypass the LLC size limit for remote CXL access.

4.2 CPU Prefetching on CXL Memory

This section presents our study of CPU prefetching on CXL memory, using both (1) software prefetching instructions which are instructions provided for programmers to hint the CPU to prefetch data, and (2) hardware prefetchers which are CPU’s built-in cache prefetchers.

Software Prefetching Instruction: The x86 ISA introduces various types of locality hints for software prefetching instructions, including T0, T1, T2, W and NTA, which fetch data to a specified location in the cache hierarchy based on the hint. According to Intel and AMD documentation, PREFETCHT0, PREFETCHW, and PREFETCHNTA bring data to the L1 cache or closer buffers, while PREFETCHT1 and PREFETCHT2 place data in the L2 cache or higher levels. PREFETCHNTA prefetches data to L1 cache in the LRU position or directly to line fill buffer (LFB) to avoid cache pollution, depending on the architecture implementation. This is useful for data that are accessed once and then discarded. PREFETCHW is a hint to the processor to prefetch data from memory into the cache in anticipation for writing.

We first measure the software prefetching latency of both CXL memory and DIMM DRAM. Figure 13a shows the latency of PREFETCHT0. On AMD-Zen4 with ASIC-CXL, the prefetching latency for the CXL memory device is 332.95 ns for local access and 414.10 ns for remote access. For DIMM, the local access time is 158.38 ns, while the remote access time is 245.47 ns. On Intel-SPR with ASIC-CXL, the CXL memory device shows 326.53 ns for local prefetching and 417.01 ns for remote prefetching. For DIMM, the local latency is 210.67 ns, and the remote latency is 256.67 ns. Compared with the load latency in Figure 2a, the performance of both CXL and DIMM software prefetching is consistent with their load latency measurements. For other prefetching hints, the latency is similar.

Next, we investigate whether the data from the CXL devices adhere to this locality mechanism. In our experiment, we first issue a prefetch instruction to fetch the data, then serialize the pipeline to ensure the prefetching completes, and finally measure the latency of a load or store on the prefetched data. The results are shown in Figure 13b. On both CXL and DIMM memory of Intel-SPR, we observe that the load/store latency after a PREFETCHT1/T2 is approximately 5ns higher than other hints, aligning with the latency difference between L1 and L2 caches. This outcome matches

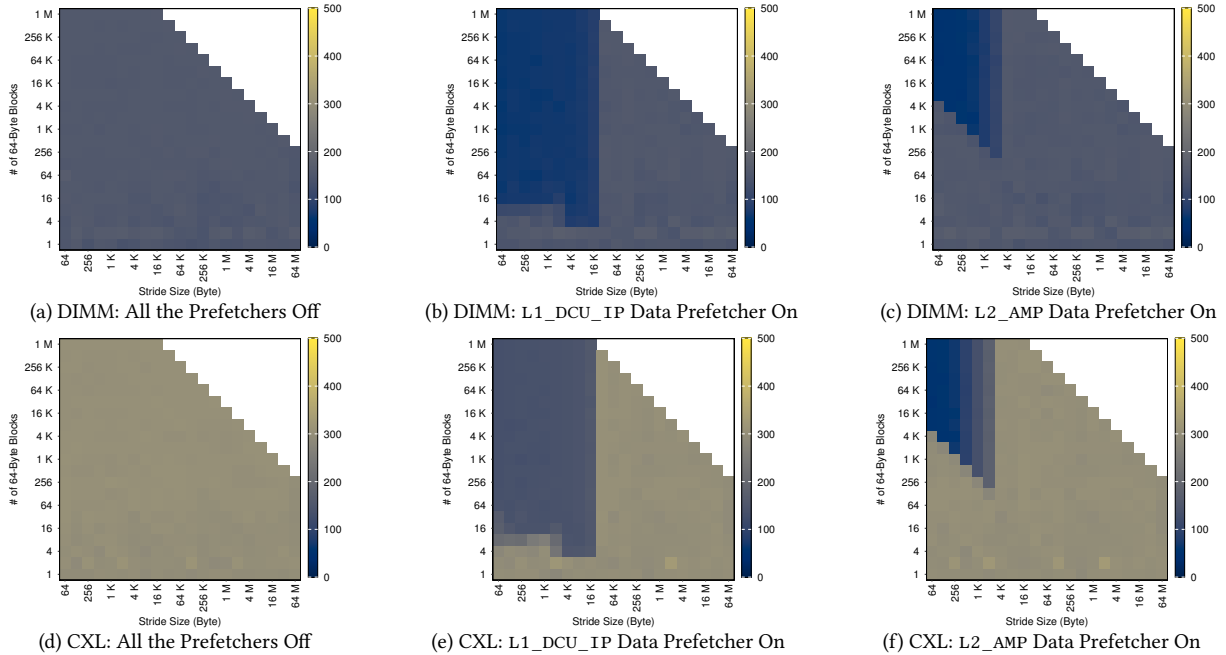


Figure 14: Hardware prefetcher footprint on Intel-SPR with ASIC-CXL

Intel’s manual [20], which states that both T1 and T2 hints bring data to the L2 cache and are implemented identically. However, on AMD-Zen4, we detect a discrepancy between CXL and DIMM memory. Specifically, the load/store latency after a PREFETCHT1/T2 on CXL data is over 20ns higher than on DIMM data. We find that on AMD-Zen4, even when serialization is added, in some cases PREFETCHT1/T2 does not fetch the data into the cache, and the data remains in CXL or DIMM memory, leading to a difference in overall average load latency. This phenomenon is not observed with other hints. In cases where PREFETCHT1/T2 successfully prefetches the data, the average load latency shows 4 cycles higher than other hints on average. This result matches what is advertised in AMD’s documentation [21] that the new feature of Zen4 is that PREFETCHT1/T2 put data into L2 cache, but we currently do not have a reason why the T1/T2 are sometimes dropped.

Hardware Prefetcher: To investigate whether the CPU hardware prefetcher performs differently during the pointer-chasing task on CXL memory, we configure the pointer-chasing access pattern to be sequential to observe the hardware prefetcher’s footprint. After each access round, we also flush all test data back to memory to minimize cache noise.

Our results indicate that most CPU hardware prefetchers maintain a consistent footprint across different memory devices on Intel-SPR with FPGA-CXL, Intel-SPR with ASIC-CXL, and AMD-Zen4 with ASIC-CXL. We illustrate two footprint examples on Intel-SPR with ASIC-CXL in Figure 14: the L1_DCU_IP and L2_AMP data prefetchers. The L1_DCU_IP prefetcher begins fetching after sequentially accessing 8 64-byte blocks each when the stride is below 4 KiB. With a stride between 4 KiB and 32 KiB, it starts prefetching after 2 blocks. For strides over 32 KiB, it stops prefetching. The L2_AMP prefetcher, on the other hand, activates after accessing 256 KiB data sequentially but prefetches only within a 4 KiB stride range. One exception we observe is that, on Intel-SPR, the L1_DCU_IP data prefetcher only prefetches data for loads to the local socket, while on AMD-Zen4, the L1 data prefetcher works for both local and remote loads. These prefetchers behave the same way when using CXL as when using DIMM.

Observation 12. CXL memory has supported both x86 software prefetching instructions and CPU hardware prefetchers, showing consistent results with DIMM DRAM.

Table 2: Intel DSA configuration.

Attribute	Value	Attribute	Value
DSA Node	0	Number of Work Queues	2
Max Batch Size (Per WQ)	32	Max Transfer Size	2 GiB

5 Accelerator Usage – Intel DSA

Intel DSA is a hardware engine for offloading memory movement and transformation operations from the CPU cores. To understand how Intel DSA compares against memcpy in latency and bandwidth, we evaluate them across local DRAM, FPGA-CXL, and ASIC-CXL on Intel-SPR. Intel DSA is configured with the parameters listed in Table 2. We use Intel DSA using Intel’s Data Movement Library (DML), and all experiments were run on Node 0.

5.1 Memory Copy Latency

To understand how Intel DSA’s latency compares against memcpy, we compare the latency of copying 512 B to 512 KiB of data using Intel DSA and memcpy. We do these experiments on a loaded and an unloaded system.

Figure 15 presents the latency comparison between Intel DSA and memcpy on a local memory node. When the data is evicted from the cache prior to the copy, DSA outperforms memcpy for transfers larger than 4 KiB. On the other hand, if the data remains cached, Intel DSA requires significantly larger transfers, around 128 KiB in our experiments, to match the performance of memcpy.

Conversely, for a loaded system running 10 parallel threads copying different data, we observe that Intel DSA performs similarly to memcpy at 16 KiB when the data isn’t cached. However, when the data is cached, Intel DSA is consistently slower than memcpy.

For slower memories, that is, the FPGA-CXL (Figure 16) and the ASIC-CXL (Figure 17), we observe that the break-even point between Intel DSA and memcpy is at 2 KiB when data is not present in the caches. If the data is already cached, memcpy consistently outperforms Intel DSA.

Further, when comparing copy latency for uncached data, we notice that regardless of the memory type, Intel DSA’s performance over memcpy improves with buffer size. For example, Intel DSA is $2\times$ faster than memcpy at 32 KiB, but $3.5\times$ at 512 KiB.

Finally, when the data being copied is available in the caches, memcpy can directly fetch the data from the caches, making it significantly faster than Intel DSA for all memory types.

Observation 13. On an unloaded system, Intel DSA can outperform memcpy for transfers larger than 4 KiB when using local DRAM and 2 KiB for CXL-based memories. However, if the data is already in the system caches, the break-even point can increase to as much as 128 KiB.

5.2 Memory Copy Bandwidth

Next, we will examine the total bandwidth achieved by Intel DSA and memcpy. For this comparison, we do not include the results for 10 threads with data eviction, as eviction introduces idle cycles for the CPU, inflating the bandwidth results.

Figure 18 compares the bandwidth achieved when copying data using Intel DSA and memcpy. With a single thread, neither Intel DSA nor memcpy can reach the peak device bandwidth as measured by Intel MLC [22]. However, with 10 simultaneous threads, Intel DSA reaches the peak bandwidth for slower memories (FPGA-CXL and ASIC-CXL), though not for the local DRAM on Intel-SPR. When data is cached, memcpy outperforms Intel DSA by a significant margin. On the other hand, when data is not cached, Intel DSA significantly outperforms memcpy.

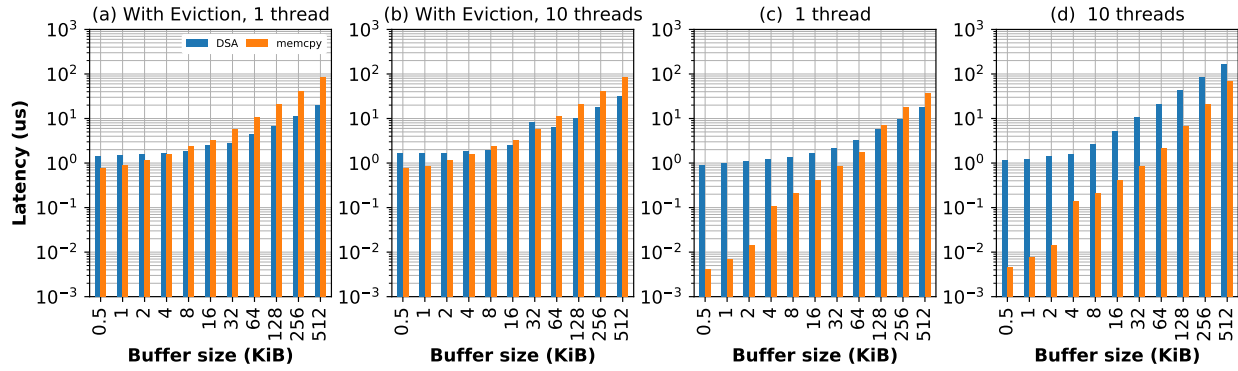


Figure 15: Latency Comparison of DRAM for 1 and 10 threads.

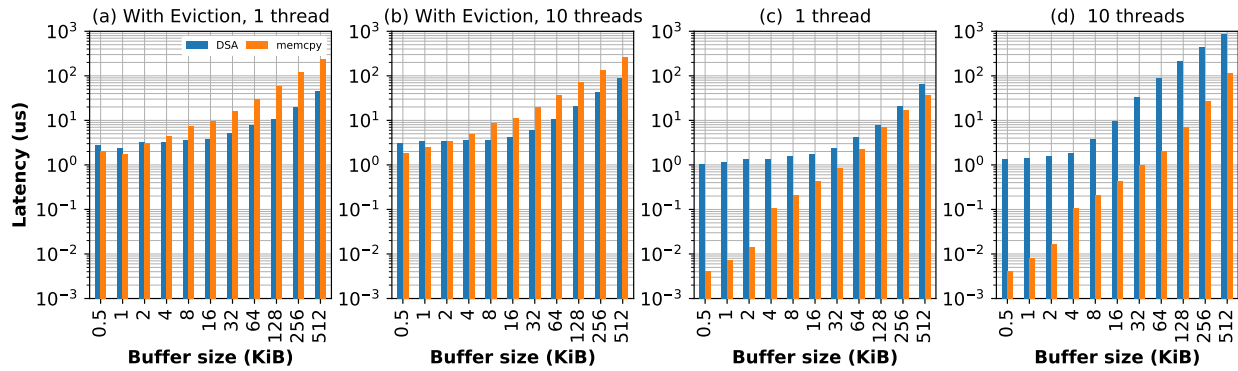


Figure 16: Latency Comparison for FPGA-CXL for 1 and 10 threads.

Observation 14. Intel DSA and memcpy require multiple threads to fully saturate the bandwidth of local memory and CXL-based memories. When the data is not cached, Intel DSA consistently delivers much higher bandwidth than memcpy, particularly for larger buffer sizes. However, when the data is cached, memcpy outperforms Intel DSA, although the performance difference narrows as the buffer size increases.

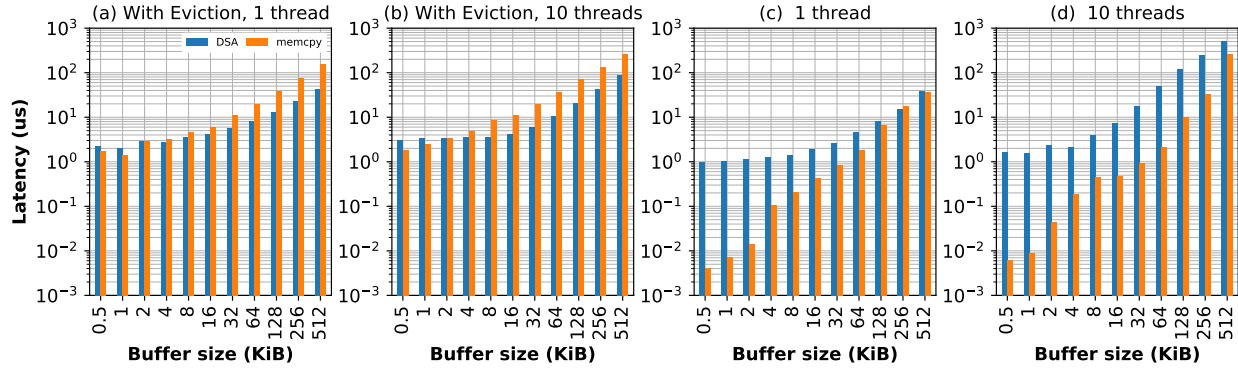


Figure 17: Latency Comparison of ASIC-CXL for 1 and 10 threads.

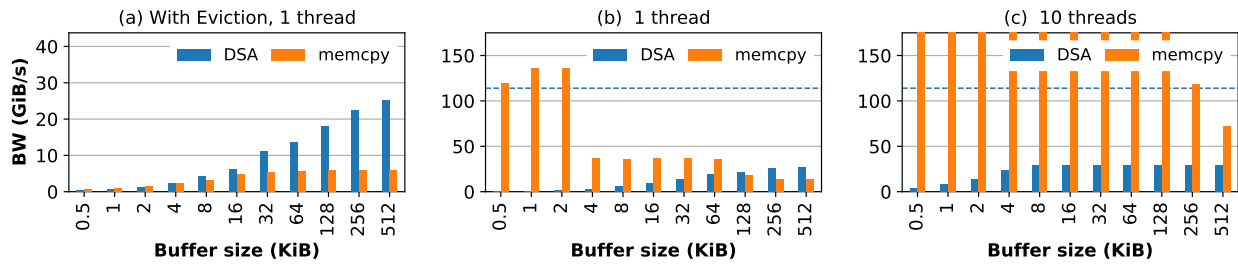


Figure 18: Bandwidth comparison for local DRAM on Intel-SPR using 1 and 10 threads. Maximum expected throughput: 114 GiB/s (blue dashed line).

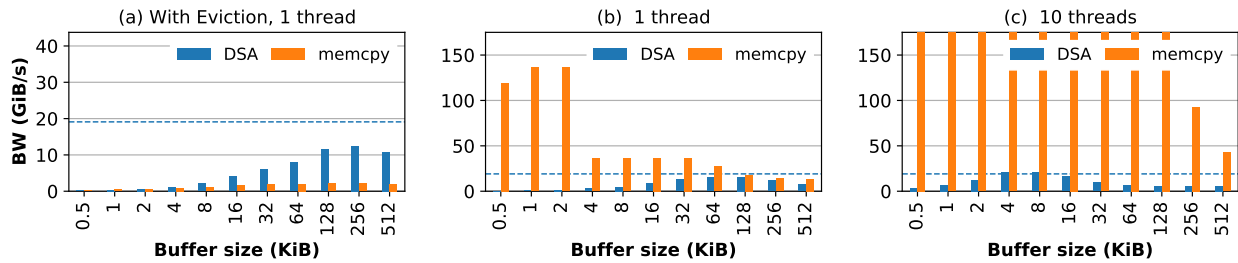


Figure 19: Bandwidth comparison for the FPGA-CXL using 1 and 10 threads. Maximum expected throughput: 19.1 GiB/s (blue dashed line).

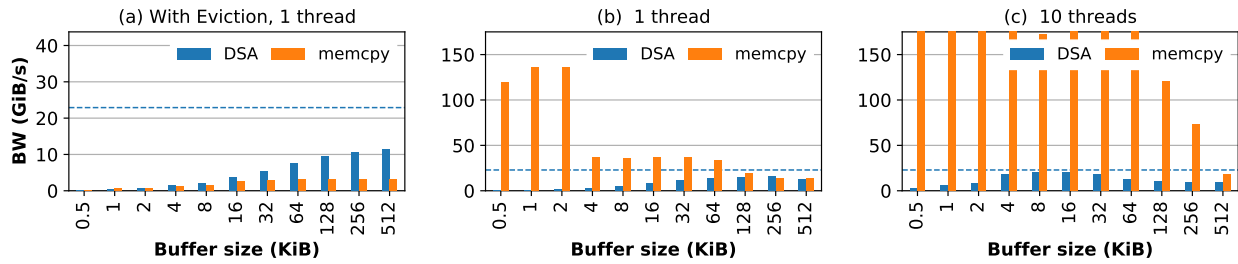


Figure 20: Bandwidth comparison for ASIC-CXL using 1 and 10 threads. Maximum expected throughput: 22.9 GiB/s (blue dashed line).

6 Applications

Based on our prior sections’ profiling of CXL system architecture and accelerator performance, we further study the application performance in such systems. In this section, we study machine learning inference, graph processing, and key-value store performance on CXL systems. We observe discrepant performance characteristics when comparing CXL vs. CPU memory as well as comparing different CXL devices. We then analyze and connect such discrepancies with our architecture-level observations to explain the application-level performance characteristics.

6.1 Machine Learning Workloads

We study the inference performance of large language models (LLMs), one of the most popular and important workloads in today’s machine learning tasks, on different CXL system configurations, using various machine learning frameworks, including PyTorch, Llama.cpp, and vLLM:

- **Meta’s Implementation with PyTorch [23]:** In this environment we use PyTorch with model files provided by the Meta’s LLaMA3 repository, including `generation.py`, `model.py`, and `tokenizer.py`. We refer to this setup as “PyTorch” in the following sections.
- **Llama.cpp [24]:** Llama.cpp is a C++ implementation of LLaMA3 inference, and we evaluate the Quantized LLaMA33 model with it.
- **vLLM [25]:** vLLM is a high-throughput and memory-efficient LLM inference engine, and we evaluate the LLaMA3 inference with it.

We use the WikiText dataset [26] in these environments whenever available. For the vLLM throughput test, we use the sharedGPT v3 dataset [27] to measure performance under modern workload conditions.

6.1.1 PyTorch with Meta’s Implementation of LLaMA3

We study the performance of Meta’s Implementation with PyTorch and use it as a baseline to compare with the following Llama.cpp and vLLM studies. In this setup, we use the testing scripts from Meta’s LLaMA3 repo [28], including the `generator` and `tokenizer` scripts to run inferences. The input data are tokenized and processed in fixed-length segments, and the processing time is measured per each input chunk. We calculate the number of tokens generated per second to evaluate the inference performance and configure the memory devices through `numactl`. We use `numactl’s cpunodebind` option to bind the PyTorch process to the CPU socket assigned to a specific NUMA memory node.

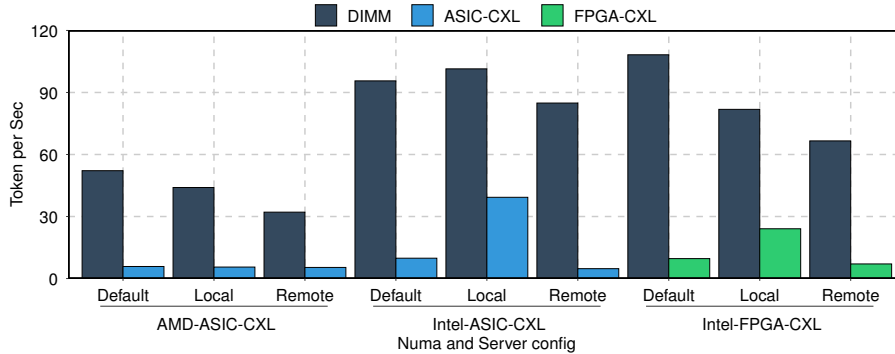


Figure 21: Token per second with PyTorch on different CXL machines. The “Default” bars show the performance with NUMA memory bind to the specific memory device, while without CPU bind (i.e., CPUs are free allocated). The “Local” and “Remote” ones have CPUs binding to corresponding CPU sockets.

Token per second measurements. Figure 21 shows our evaluation of LLaMA3 inference performance with PyTorch using different CXL machines. We first observe that inference with DRAM-only is generally faster than CXL memory, and among different CXL memory devices, ASIC-CXL is usually faster than FPGA-CXL, with an exception that using remote FPGA-CXL on Intel-SPR is faster than remote ASIC-CXL. It is likely caused by the lower efficiency when

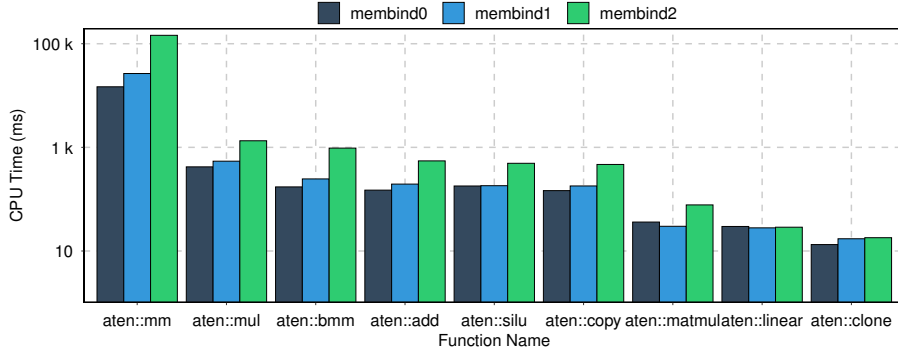


Figure 22: PyTorch profiler's results on Intel-SPR with FPGA-CXL.

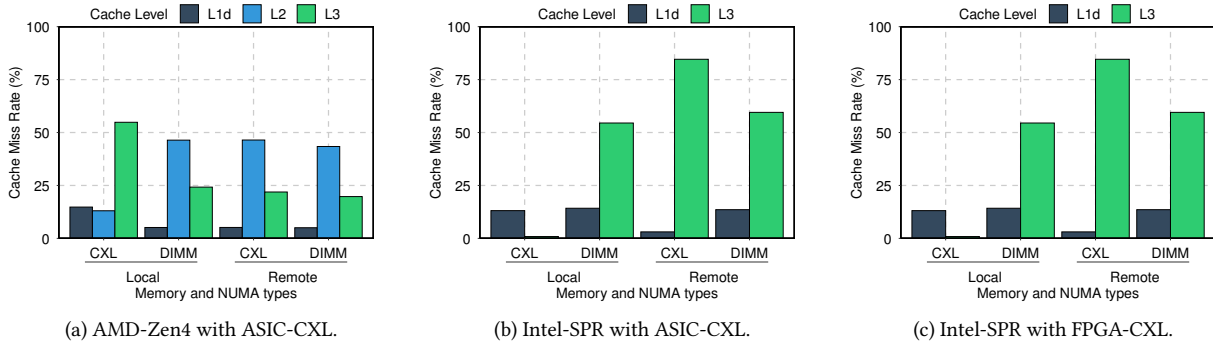


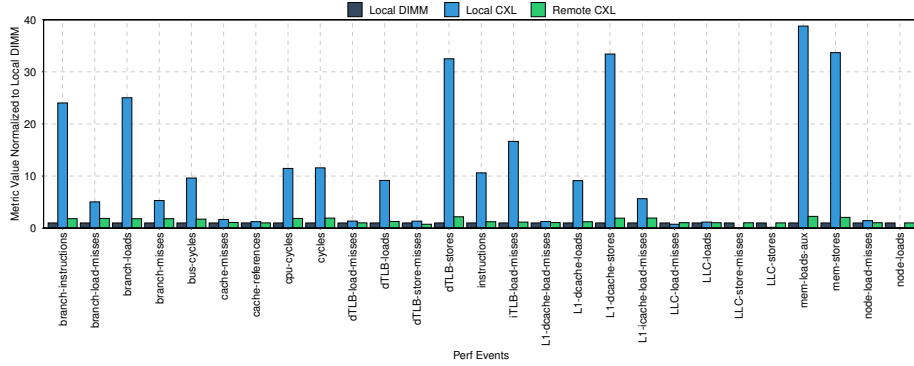
Figure 23: Cache miss rate different machines. The Local CXL's L3 cache events are not properly reported by the Linux Kernel and perf tool we used. We believe this is a bug in the Linux kernel source code and will revise the result once the kernel fixes it.

using ASIC-based CXL memory expander on the remote socket, due to lack of native support of CXL.mem protocol with the current generation of Intel-SPR CPUs. In this case, the FPGA-based CXL.mem implementation may leverage Intel's in-house optimizations in their FPGA CXL IP to provide better remote access performance.

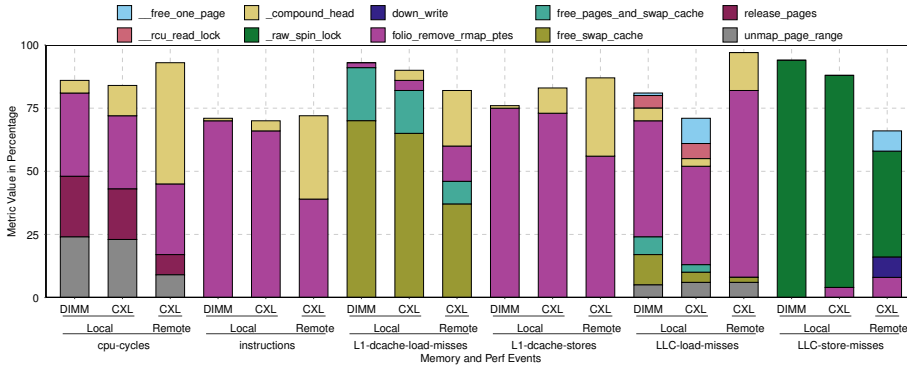
When using different CPU binding settings, we find that with Intel-SPR and ASIC-CXL, binding CPUs (*Local* and *Remote*) offers higher performance using DRAM, than allowing CPUs to be freely allocated on both sockets (*Default*). As shown in Figure 21, binding Intel-SPR CPU for local CXL access performs significantly better than other settings. This indicates that binding CPUs through `numactl` helps PyTorch to better schedule tasks and allocate memory when using slower devices such as CXL memory. In contrast, we do not observe similar performance characteristic on AMD-Zen4, whose overall performance is lower than Intel-SPR, potentially because PyTorch under-utilizes the CPU and memory performance on AMD-Zen4.

Function-level profiling. We use PyTorch profiler to get high-level performance characteristics of the LLaMA3 inference. The tool reports the execution time of each internal functionality. As shown in Figure 22, using CXL memory incurs significantly longer execution time for memory-intensive operations, especially in matrix multiplication functions including `aten::mm`, `aten::matmul`, and `aten::mul`. These operations access the matrix data stored in off-core memory and incur longer execution time if CXL memory is used instead of DRAM.

Profiling cache miss rates. We profile the cache miss rate each inference environment to further study the inference performance. We use `perf` [12] on Intel CPUs and `AMD uProf` [13] on AMD CPUs to extract cache-related hardware counters. As shown in Figure 23, we find that CXL incurs higher L3 cache miss rates in all of our settings, except for local CXL access on Intel-SPR, where the L3-related hardware counters are not properly reported due to bugs in `perf` and Linux kernel. In addition, we find that when using CXL memory on Intel-SPR CPU, remote CXL has a higher L3 cache miss rate than remote DIMM, and the gap is larger than that on AMD-Zen4. We conclude that this



(a) Performance counters compared to the local DIMM setup.



(b) Breakdown of cache-related perf events.

Figure 24: Performance profiling results when running LLaMA3 inference with PyTorch on Intel-SPR with FPGA-CXL.

is highly related to the limited L3 cache size for remote CXL access, as described in Section 4.1.4. It also contributes to Intel-SPR’s lower inference performance when using remote CXL compared to remote DIMM, as shown in Figure 21. We expect the cache miss rate with CXL to be similar to using DIMM because we infer the same model with the same inference engine, while in fact, local CXL on AMD-Zen4 and remote CXL on Intel-SPR have higher L3 miss rates. Therefore, our conclusion is that the inference framework would need extra optimizations to reduce the miss rates on CXL.

Observation 15. CXL can cause higher cache miss rates even with the same model inference on the same framework.

In-depth profiling. Besides the cache miss rate, we also take an in-depth analysis of other performance events during the LLaMA3 inference. We run the inference with 128-token chunks and capture CPU and memory performance events from *perf* on the Intel-SPR with FPGA-CXL. The memory access patterns were fixed by binding CPU and memory to specific NUMA nodes and profiling each setting’s performance counters. This allows us to isolate the overheads associated with different memory access strategies. Specifically, we record *perf* events related to the inference process and visualize the overhead ratios across different memory devices. Figure 24 shows our profiling results, where Figure 24a shows the performance counter values normalized to the local DIMM setup, and Figure 24b shows the breakdown of selected cache-related perf events.

From Figure 24a we find that using CXL memory incurs significantly higher overheads of a few perf events, including the number of branch instructions, dTLB stores, L1 dcache stores, and main memory load and stores. We conclude that the higher number of branch instructions is caused by the use of spin lock with CXL memory, where the execution of atomic instructions is significantly slower on CXL memory than DRAM, causing spin lock to execute excessive conditional branches and wasting CPU cycles. We build a proof-of-concept spin lock (Section 3.6) using CXL and

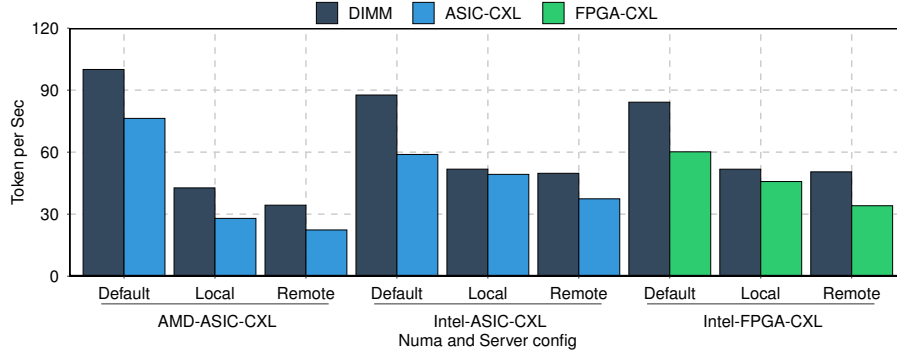


Figure 25: Token per second with during Llama.cpp inference.

DRAM to demonstrate this effect and prove our hypothesis. Additionally, the LLC store misses are dominated by `_raw_spin_lock` as shown in Figure 24b, indicating that spin lock is wasting CPU cycles and memory transfers. This spinlock can busy-wait for a long time and potentially block other processes to get a fair share of CPU time, hurting the overall system performance.

Observation 16. Spinlock incurs significant overhead when using CXL memory. A program may choose to either (1) use other types of locks to yield CPU time to other processes or (2) lower the frequency of atomic instruction usage.

We further break down the cache-related performance events to the function level and present the functions that dominate each event. As shown in Figure 24b, CXL generally has the same function breakdown distribution compared to local and remote DRAM. In other words, the percentage of each function’s execution time in an event remains similar to that of DRAM, even though CXL’s event has a higher absolute value.

Looking closer, we find that `folio_remove_rmap_ptes()` function dominates the *instructions*, *L1-dcache-stores*, and *LLC-load-misses* events. This function [29] removes all reverse mapping entries associated with a given folio’s page table entries (PTEs). Doing so ensures that the kernel no longer maintains references from the PTEs to the physical pages within that folio, which is crucial during operations like unmapping memory regions or freeing up pages. This process involves excessive memory access and synchronization, thus dominating the aforementioned performance events. Additionally, when the page table is stored in CXL memory, this function significantly impacts the overall program performance, motivating the need to use memory-tiring systems or statically avoid allocating page tables on CXL to reduce overhead.

For the *cpu-cycles* and *L1-dcache-stores* events, they have a high absolute metric value when using CXL (Figure 24a), but their distribution (Figure 24b) remain similar across three different memory, indicating that using CXL for LLAMA3 inference does not impact much on code execution pattern or CPU L1 dcache access pattern.

6.1.2 Llama.cpp

In this section, we evaluate the performance of the language model using a perplexity benchmark in the llama.cpp environment. Specifically, the model used is Meta-Llama-3-8B.Q4_K_M.gguf, with 8.03 billion parameters in GGUF V3 format. The perplexity benchmark is run using the WikiText dataset, with a context length of 512 tokens, a batch size of 2,048 tokens, and a sequence count of 4. We also enable SMT threads and SIMD optimizations to fully utilize the hardware resources.

Figure 25 shows the tokens-per-second performance under different memory and CPU binding configurations on both Intel-SPR and AMD-Zen4 CPUs. If “local” or “remote” is specified, we bind the model to one CPU socket and allocate all the data in its “local” or “remote” memory devices. Otherwise, no binding is enabled, and all sockets and memory devices are utilized.

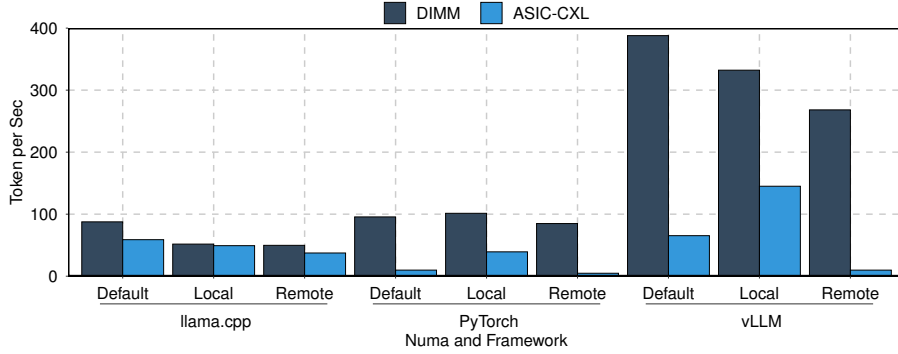


Figure 26: Token per second comparison between three frameworks, all on the Intel-SPR with ASIC-CXL.

Compared to PyTorch Inference of LLaMA, Llama.cpp shows less performance degradation when using CXL memory. When binding the model to one socket, Intel-SPR performs better on both DIMM and CXL. However, when running without socket binding—allowing the model to utilize both sockets—AMD-Zen4 outperforms Intel-SPR on both DIMM and CXL. Specifically, AMD-Zen4 achieves up to a 191.97% increase in performance on DIMM and a 241.11% increase on CXL. In contrast, Intel-SPR scales less efficiently with more computing resources, with a performance increase of only 66.76% on DIMM and 75.50% on CXL. This suggests that AMD-Zen4 benefits from better socket interconnect performance and a more efficient scheduling policy, consistent with the findings of Section 3.2.

For local and remote access comparison, on Intel-SPR, the performance difference on DIMM memory is slight (Local 51.76 vs. Remote 50.48, a 2.47% decrease). In contrast, on AMD-Zen4, there is a 19.59% decrease on the remote DIMM. However, when using remote CXL, Intel-SPR shows a much larger performance drop (25.55%) compared to AMD-Zen4 (19.98%). This larger drop on Intel-SPR could be due to lower bandwidth and a smaller usable LLC size for remote CXL accesses, as shown in previous sections.

When comparing socket binding and no binding, unlike PyTorch inference, using CXL without socket binding even outperforms using local DIMM or remote DIMM with binding. This suggests that the Llama.cpp workload is more sensitive to CPU resource availability than to memory latency.

6.1.3 vLLM

In this section, we evaluate another inference framework, vLLM: a library and platform designed for efficient inference and serving of LLMs. vLLM is widely recognized for its memory-efficient operations, which guarantees high performance by optimizing memory utilization and batching requests. We deploy the same Llama3 8B model and run the benchmark_throughput.py script provided by the library on the Intel-SPR with ASIC-CXL. The dataset is ShareGPT_v3. The key value (KV) cache size is set to 30 GiB. We use the same measurement as in previous sections and compare different memory and CPU configurations.

The results are presented in Section 6.1.3. We observe a much higher throughput on vLLM than on Pytorch and llama.cpp on DIMM and local CXL. Local CXL shows a decrease of around 60% compared to local DIMM, which is similar to their difference in latency. However, remote CXL shows significantly lower performance, with a throughput of only 9.81 tokens per second. This indicates that besides latency, cache size and bandwidth limits could also impact remote CXL performance. This also harms performance under the default strategy (without CPU binding), because some threads access the CXL memory from the remote socket. This shows that vLLM is sensitive not only to memory latency but also to bandwidth and CPU cache size.

These results suggest that when running vLLM on CXL memory on the Intel-SPR, applying CPU binding to the local socket can mitigate performance drops caused by remote CXL access. In contrast, for DIMM configurations, maximizing CPU utilization without CPU binding can achieve better performance.

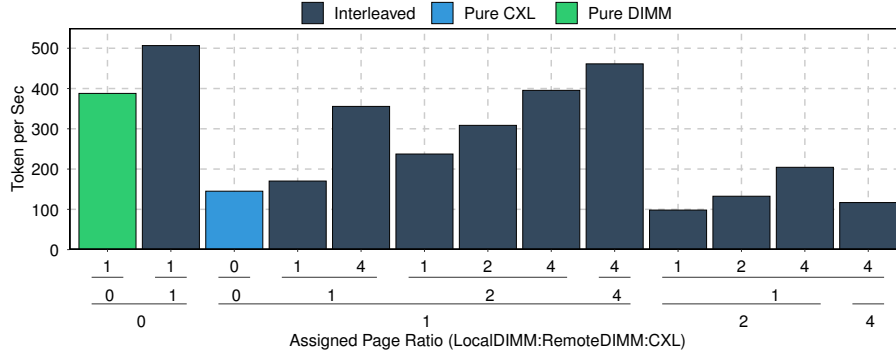


Figure 27: vLLM token per second with different weighted interleaving settings on Intel-SPR with ASIC-CXL. The X-axis shows the page assignment ratio, which, from top to bottom, represents local DIMM, remote DIMM, and local CXL. We interleave the memory while allowing CPU processes to be freely allocated across both CPU sockets.

6.1.4 Weighted interleave

We study the vLLM performance on the Intel-SPR with ASIC-CXL by enabling the weighted interleave through the `numactl` option. The weighted interleave feature allows memory to be assigned, stored, and accessed across various NUMA nodes in proportions specified by assigned weights. In contrast, traditional interleaving distributes memory access evenly in a round-robin fashion across nodes. We have studied the interleaving bandwidth with microbenchmarks in Section 3.4 and this section focus on vLLM inference when using weighted interleaving.

As shown in Figure 27, we find that using pure DRAM, especially when using DRAM DIMM from both sockets, achieves higher tokens per second than using pure CXL memory, which aligns with our results in Section 3.4. In addition, interleaving both DIMM and CXL achieves higher performance than using only the CXL, where the 4:4:1 config (four pages on local DIMM, four on remote DIMM, and one on local CXL) achieves nearly the peak DIMM bandwidth. Since this system only has one memory expander, we expect the optimal configuration to change when more expanders are added.

We also find that the weighted interleaving may not fully utilize the system’s aggregated bandwidth, where the added CXL bandwidth should help achieve higher than pure DIMM bandwidth. This is potentially due to the machine learning inference framework not specifically optimized to utilize the added CXL bandwidth, and also the interleaving scheme does not consider the memory access pattern. While achieving sub-optimal performance, the weighted interleaving is a drop-in solution, i.e., not requiring any software change, to expand the total memory capacity. We envision that weighted interleaving could serve as an early exploration of software that uses CXL memory and later guide the optimization strategies to fully utilize the total bandwidth.

6.2 Vector DB

Vector databases are built for managing and querying high-dimensional data, which is essential in applications involving machine learning and AI. These systems store vector embeddings—mathematical representations of data such as text, images, and audio generated by machine learning models. By leveraging vector similarity search, they enable efficient retrieval of data which is important for tasks such as recommendation systems, image similarity searches, and natural language processing. We use two vector databases, Qdrant [30] and Milvus [31], to evaluate the CXL performance impact relative to DIMM performance. Our goal is to understand how CXL handles high-throughput, real-time similarity search workloads and the impact on Requests Per Second (RPS), precision, and latency (p95 and p99) relative to DIMM. We use *glove100* [32] as the input for both vector databases, which includes pre-trained global vectors for word representation (GloVe) for approximate neighbor search.

Figure 29 shows the results for Intel-CXL, AMD-CXL, and Intel-FPGACXL. Across the three systems, DIMM achieved up to $3.5\times$ higher RPS than CXL, with the Intel-CXL machine showing the smallest RPS difference between DIMM and CXL. For the two other machines, we see a similar trend in the CXL performance. Regarding latency, the p95 and p99 latencies are below 0.1ms for DIMM across all systems, while the CXL latencies in the Intel-CXL machine show

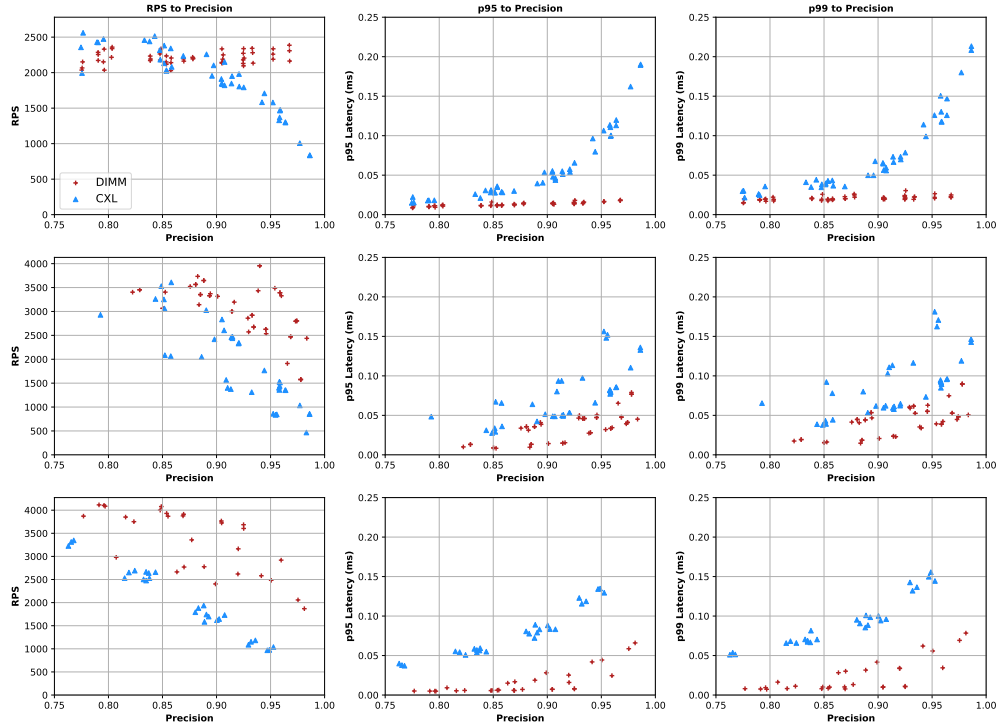


Figure 28: Milvus RPS, p95 and p99 results for Intel-CXL, AMD-CXL and Intel-FPGACXL machines.

Table 3: Graph and KV workloads

Workload	Description
graph_gen	Graph generation with 50M vertices and 250M edges
pagerank	Pagerank algorithm on the generated graph
bfs	BFS algorithm on the generated graph
local_clustering	Local clustering algorithm on the generated graph
redis_sets	50M SET operations on redis
redis_gets	50M GET operations on redis
memcached_sets	50M SET operations on memcached
memcached_gets	50M GET operations on memcached

the best performance. On the other hand, the AMD-CXL and Intel-FPGACXL machines show similar CXL latencies, with an up to $8\times$ increase for both latencies.

In Figure 28, across all three machines, we observe that DIMM and CXL have similar performance in terms of RPS, with the CXL performance dropping faster as the precision increases. In addition, the Intel-CXL machine achieves the smallest max RPS for both DIMM and CXL. Regarding latency, all systems display similar p95 and p99 latencies, with the Intel-CXL machine having the lowest latency for DIMM, and Intel-FPGACXL displaying the lowest p99 latency for CXL.

In conclusion, we notice that the performance of each vector database varies and depends heavily on the underlying system, including the CPU and CXL architecture. For Qdrant, the Intel-CXL and AMD-CXL machines offer better performance, while Milvus achieves the best performance for the Intel-FPGACXL machine.

6.3 Graph and Key-Value Workloads

This section contains the performance of four graph (*graph generation*, *pagerank*, *local clustering*, *BFS*) and four KV workloads (*redis SET*, *redis GET*, *memcached SET*, *memcached GET*). Table 3 contains the graph and KV workloads that

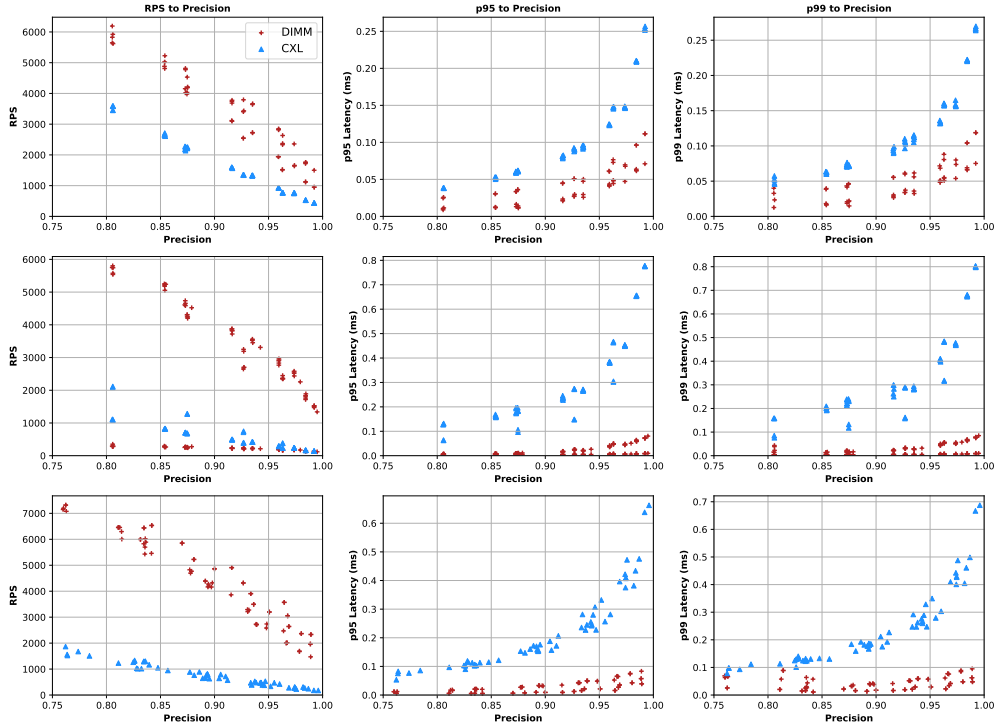


Figure 29: Qdrant RPS, p95 and p99 results for Intel-CXL, AMD-CXL and Intel-FPGA CXL machines.

we used for our evaluation on Intel’s and AMD’s DRAM and CXL. We run these benchmarks on bare metal and a virtual machine, while we also present the results for using base pages (4 KiB) and huge pages (2 MiB) on bare metal. For all experiments we measure the execution time 5 times and report the normalized average execution time.

We use QEMU/KVM [33] version 4.2.1 to spawn and manage virtual machines (VMs) in our experimental setup. For the graph workloads we use the graph-tool module in Python and for the KV workloads we are using the redis (redis-py) and memcached (python-memcached) python clients [34, 35].

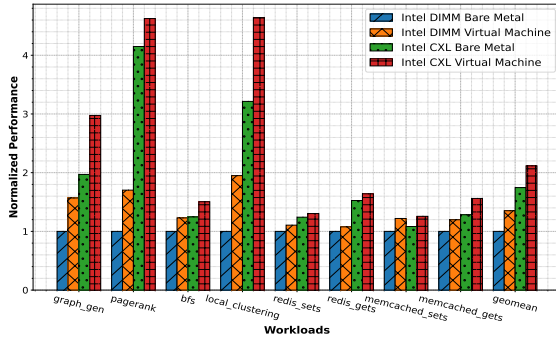
6.3.1 Bare Metal and Virtual Machine performance

Figures 30a, 31a and 32a show the performance for the 8 workloads that we run on bare metal and on a virtual machine, plus the geomean of all workloads. The performance is normalized against the baseline, which is each server’s DIMM bare metal performance. We have the following observations: **First**, the VM overhead over the bare metal execution is proportional for both DIMM and CXL in most workloads, with the AMD-CXL machine having the lowest VM performance degradation. **Second**, the graph workloads have a worse performance overhead with CXL than the KV workloads. This is expected as the former are more memory intensive, with *pagerank* and *local_clustering* incurring the highest performance overhead. **Third**, the best CXL performance is achieved by Intel-CXL with AMD-CXL and Intel-FPGACXL showing similar performance.

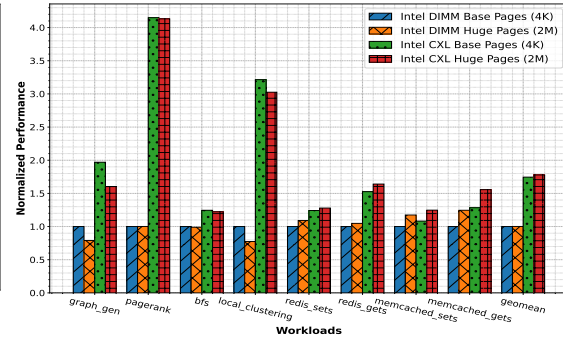
6.3.2 Bare Metal and Virtual Machine performance

Figures 30b, 31b and 32b presents the performance of 8 different workloads, along with the geometric mean, using both base pages (4 KiB) and huge pages (2 MiB). The performance is normalized against the baseline, which is each server’s DIMM bare metal with 4 KiB pages performance.

We have the following observations: **First**, we notice that the use of 2MiB pages has a different performance impact in each machine. The Intel-CXL’s geomean shows a similar performance between the two different page sizes, while the AMD-CXL’s geomean shows a 60% performance degradation when using CXL with huge pages. Last, the Intel-FPGACXL’s geomean shows similar performance improvement in DIMM and DRAM with 2 MiB pages. **Second**, we

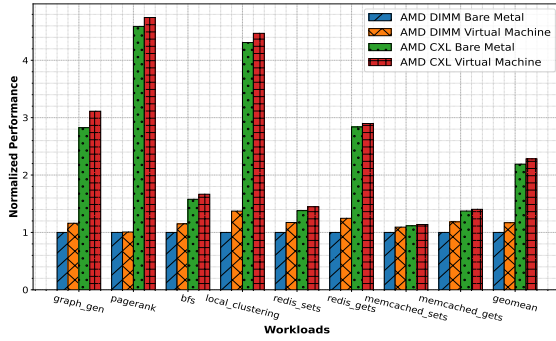


(a) Bare metal and VM normalized performance.

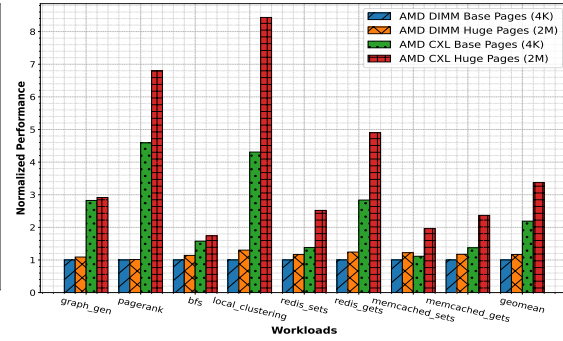


(b) 4KiB and 2MiB normalized performance.

Figure 30: Normalized performance for graph and KV workloads on Intel-DIMM and Intel-CXL.



(a) Bare metal and VM normalized performance.



(b) 4KiB and 2MiB normalized performance.

Figure 31: Normalized performance for graph and KV workloads on AMD-DIMM and AMD-CXL.

notice that again the worst performance degradation appears in graph workloads, due to their memory intensiveness. **Third**, the CXL performance degradation with 2 MiB pages in some cases is bigger proportionally compared to the DIMM's 2 MiB overhead (e.g. *pagerank* in AMD-CXL).

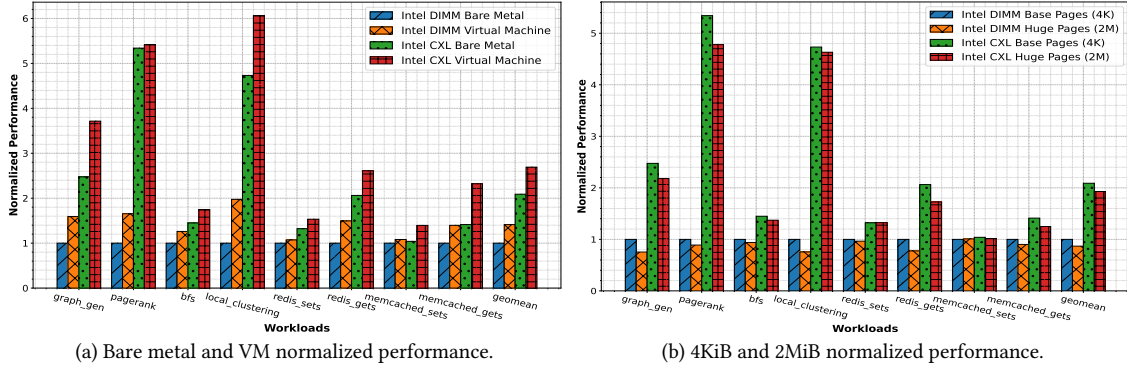


Figure 32: Normalized performance for graph and KV workloads on Intel-DIMM and Intel-FPGA CXL.

7 Related Work

Several recent studies explored CXL-based systems’ characteristics, performance, and programmability.

Performance Characterization. Sun et al. [18] evaluate several real and emulated CXL devices. They show that (a) real CXL devices can have better performance than NUMA-emulated CXL in some cases, (b) latency-sensitive applications suffer from CXL’s higher access latency, and (c) propose a mechanism for dynamically tiering pages between DRAM and CXL devices. Liu et al. [36] compare and contrast CXL-attached memory devices with traditional DRAM-based NUMA node, explore use cases for CXL given its higher access latency compared to locally-attached DRAM, and go beyond Sun et al. and show that several HPC workloads can tolerate CXL-attached memory’s high latency and low throughput. They also observed limited performance improvements in GPU LLM workloads when offloading tensors to CXL-attached memory. Tang et al. [37] evaluate the performance of CXL for cloud workloads and develop a model to estimate CXL’s total cost of ownership (TCO). Previous works have also characterized other memory devices that offer an interface similar to CXL-attached memory [38–40].

Memory Bandwidth and Capacity Expansion. Pond [41] proposes a multi-host memory pooling solution to help with stranded memory in production cloud workloads. They show that a significant number of workloads show negligible performance loss when their entire memory is allocated in the memory pool. Levis et al. [42], however, argues against memory pooling for cloud workloads because of their cost, complexity, and utility. Yang et al. [43] evaluate a new DRAM-SSD hybrid CXL-based memory pooling architecture and show promising results for HPC workloads. Wahlgren et al. [44] developed a profiler for studying HPC workloads’ memory access pattern and study capacity and bandwidth provisioning. Zhong et al. [45] developed a CXL memory allocator to intelligently allocate and place VM pages in multi-tenant hosts, minimizing workload slowdown. Transparent page placement (TPP) [9] is a mechanism to proactively place workload’s cold pages in the far memory to enable faster near-memory allocations when new requests arrive. TPP can also dynamically and transparently move application pages between the near- and far-memory based on their *hotness*. TPP is submitted to be upstreamed into Linux [46]. Berger et al. [47] explore the design space of CXL-based memory pools and draw recommendations. They also study the cost savings from different pool sizes and find small pools to be the most cost-effective.

Adapting applications for CXL. Previous works have also looked at the performance of a number of applications on CXL. CC-NIC [48] implements a custom Host-NIC interface to take advantage of the CXL’s byte-addressability and coherency, resulting in reduced latency and higher throughput compared to today’s PCIe NICs. Other works [49–51] implement RPCs over CXL take advantage of the cache-coherent interface, improving performance. Many research works have also looked into CXL-enabled persistence [52–56]. Cabrera et al. [57] propose the use of CXL in heterogeneous accelerator systems to enable easier and fine-grained collaboration as opposed to host-enabled memory sharing.

Āpta [58] uses CXL-disaggregated memory to implement fault-tolerant object stores for function-as-a-service workloads outperforming RDMA-based solutions. Wei et al. [59] make a case for transaction index over CXL-based

distributed memory using a lightweight distributed memory transaction primitive (rTX). rTX achieves significant performance improvement over other transactional indexes while minimizing the overhead of failure atomicity. Aralakis et al. [60] propose a CXL-attached memory expander that implements on-the-fly compression/decompression for hyperscalar workloads. They propose this as an alternative to software-based memory compression, saving CPU cycles.

8 Acknowledgement

The authors thank Hoshik Kim and Jongryool Kim for their valuable feedback. We also thank Kevin Xue for his contribution to this work. This paper is supported by the PRISM and ACE centers in JUMP 2.0, an SRC program sponsored by DARPA.

9 Conclusion

In this paper, we develop a memory benchmark suite, HEIMDALL, and leverage it to study a wide range of CXL-attached systems' performance. Our observations span across the system architecture stack, from basic hardware behaviors, to micro-architecture and operating system performance, and applications including LLM inference and vector databases. These observations shed light on the future development of heterogeneous memory architecture and optimization in system software to better utilize such memory systems.

References

- [1] Denis Foley and John Danskin. “Ultra-Performance Pascal GPU and NVLink Interconnect”. In: *IEEE Micro* 37.2 (2017), pp. 7–17.
- [2] Intel Corporation. *Intel® Xeon® Processor Scalable Family Technical Overview*. <https://www.intel.com/content/www/us/en/developer/articles/technical/xeon-processor-scalable-family-technical-overview.html>. Updated 12/1/2022, Accessed: 2024-10-14. 2022.
- [3] Gabin Schieffer, Ruimin Shi, Stefano Markidis, Andreas Herten, Jennifer Faj, and Ivy Peng. *Understanding Data Movement in AMD Multi-GPU Systems with Infinity Fabric*. 2024. arXiv: 2410.00801 [cs.DC]. URL: <https://arxiv.org/abs/2410.00801>.
- [4] CXL Consortium. *CXL Consortium releases Compute Express Link 3.0 specification*. URL: <https://www.computeexpresslink.org/pressroom>.
- [5] Gen-Z Consortium. *The Gen-Z Consortium*. URL: <https://genzconsortium.org/>. (accessed: 06.24.2020).
- [6] CCIX Consortium. *CCIX*. URL: <https://www.ccixconsortium.com/>. (accessed: 06.24.2020).
- [7] Ying Wei, Yi Chieh Huang, Haiming Tang, Nithya Sankaran, Ish Chadha, Dai Dai, Olakanmi Oluwole, Vishnu Balan, and Edward Lee. “NVLink-C2C: A Coherent Off Package Chip-to-Chip Interconnect with 40Gbps/pin Single-ended Signaling”. In: *2023 IEEE International Solid-State Circuits Conference (ISSCC)*. 2023.
- [8] Ira Weiny. *cxl/pci: Skip irq features if MSI/MSI-X are not supported*. URL: <https://lore.kernel.org/lkml/t6wkohozmtchuzzabjigr66tx6576nni54ig7lu2orlvqwm5o@r52mxzei7uxs/T/>.
- [9] Hasan Al Maruf, Hao Wang, Abhishek Dhanotia, Johannes Weiner, Niket Agarwal, Pallab Bhattacharya, Chris Petersen, Mosharaf Chowdhury, Shobhit Kanaujia, and Prakash Chauhan. “TPP: Transparent Page Placement for CXL-Enabled Tiered-Memory”. In: *Proceedings of the 28th ACM International Conference on Architectural Support for Programming Languages and Operating Systems*. ASPLOS 2023. 2023.
- [10] Intel. *Technical Overview Of The 4th Gen Intel Xeon Scalable processor family*. URL: <https://www.intel.com/content/www/us/en/developer/articles/technical/fourth-generation-xeon-scalable-family-overview.html>.
- [11] AMD. *4th Gen AMD EPYC Processor Architecture*. URL: <https://www.amd.com/en/products/processors/server/epyc/4th-generation-architecture.html>.
- [12] Brendan Gregg. *Linux Perf Examples*. 2024. URL: <http://www.brendangregg.com/perf>.
- [13] AMD. *AMD µProf*. 2024. URL: <https://www.amd.com/en/developer/uprof.html>.
- [14] Intel. *Intel Performance Counter Monitor*. URL: <https://github.com/intel/pcm>.
- [15] *Intel® 64 and IA-32 Architectures Optimization Reference Manual Volume 1*. URL: <https://www.intel.com/content/www/us/en/content-details/671488/intel-64-and-ia-32-architectures-optimization-reference-manual-volume-1.html>.
- [16] Intel. *Intel Data Direct I/O Technology*. URL: <https://www.intel.com/content/www/us/en/io/data-direct-i-o-technology.html>.
- [17] Alireza Farshin, Amir Roozbeh, Gerald Q Maguire Jr, and Dejan Kostić. “Reexamining Direct Cache Access to Optimize {I/O} Intensive Applications for Multi-hundred-gigabit Networks”. In: *2020 USENIX Annual Technical Conference (USENIX ATC 20)*. 2020, pp. 673–689.
- [18] Yan Sun, Yifan Yuan, Zeduo Yu, Reese Kuper, Chihun Song, Jinghan Huang, Houxiang Ji, Siddharth Agarwal, Jiaqi Lou, Ipoom Jeong, et al. “Demystifying CXL memory with genuine CXL-ready systems and devices”. In: *Proceedings of the 56th Annual IEEE/ACM International Symposium on Microarchitecture (MICRO)*. 2023.
- [19] *Introduction to Cache Allocation Technology in the Intel® Xeon® Processor E5 v4 Family*. URL: <https://www.intel.com/content/www/us/en/developer/articles/technical/introduction-to-cache-allocation-technology.html>.
- [20] Intel. *Intel 64 and IA-32 Architectures Software Developer Manuals*. URL: <https://www.intel.com/content/www/us/en/developer/articles/technical/intel-sdm.html>.

- [21] AMD. *AMD64 Architecture Programmer's Manual, Volumes 1-5*. URL: <https://www.amd.com/en/support/tech-docs>.
- [22] Intel® *Memory Latency Checker v3.11a*. URL: <https://www.intel.com/content/www/us/en/developer/articles/tool/intelr-memory-latency-checker.html>.
- [23] Jason Ansel, Edward Yang, Horace He, Natalia Gimelshein, Animesh Jain, Michael Voznesensky, Bin Bao, Peter Bell, David Berard, Evgeni Burovski, Geeta Chauhan, Anjali Chourdia, Will Constable, Alban Desmaison, Zachary DeVito, Elias Ellison, Will Feng, Jiong Gong, Michael Gschwind, Brian Hirsh, Sherlock Huang, Kshiteej Kalambarkar, Laurent Kirsch, Michael Lazos, Mario Lezcano, Yanbo Liang, Jason Liang, Yinghai Lu, C. K. Luk, Bert Maher, Yunjie Pan, Christian Puhersch, Matthias Reso, Mark Saroufim, Marcos Yukio Siraichi, Helen Suk, Shunting Zhang, Michael Suo, Phil Tillet, Xu Zhao, Eikan Wang, Keren Zhou, Richard Zou, Xiaodong Wang, Ajit Mathews, William Wen, Gregory Chanan, Peng Wu, and Soumith Chintala. "PyTorch 2: Faster Machine Learning Through Dynamic Python Bytecode Transformation and Graph Compilation". In: *Proceedings of the 29th ACM International Conference on Architectural Support for Programming Languages and Operating Systems, Volume 2*. ASPLOS '24. 2024.
- [24] Georgi Gerganov. *LLama.cpp: Port of Meta's LLaMA model to C/C++*. GitHub repository. 2023. URL: <https://github.com/ggerganov/llama.cpp>.
- [25] Woosuk Kwon, Zhuohan Li, Siyuan Zhuang, Ying Sheng, Lianmin Zheng, Cody Hao Yu, Joseph E. Gonzalez, Hao Zhang, and Ion Stoica. "Efficient Memory Management for Large Language Model Serving with PagedAttention". In: *Proceedings of the ACM SIGOPS 29th Symposium on Operating Systems Principles*. 2023.
- [26] Stephen Merity, Caiming Xiong, James Bradbury, and Richard Socher. *Pointer Sentinel Mixture Models*. 2016. arXiv: 1609.07843 [cs.CL].
- [27] OpenChat. *OpenChat ShareGPT V3 Dataset*. Accessed: 2024-11-01. 2024. URL: https://huggingface.co/datasets/openchat/openchat_sharegpt_v3.
- [28] Hugo Touvron, Thibaut Lavril, Gautier Izacard, Xavier Martinet, Marie-Anne Lachaux, Timothée Lacroix, Baptiste Rozière, Naman Goyal, Eric Hambro, Faisal Azhar, Aurelien Rodriguez, Armand Joulin, Edouard Grave, and Guillaume Lample. "LLaMA: Open and Efficient Foundation Language Models". In: *arXiv preprint arXiv:2302.13971* (2023). URL: <https://arxiv.org/abs/2302.13971>.
- [29] Linus Torvalds. *Linux kernel*. URL: <https://github.com/torvalds/linux/blob/6c52d4da1c742cd01a797a4d0a2d3c5a60dc9bfe/mm/rmap.c#L1609gg>.
- [30] qdrant. *Qdrant: High-Performance Vector Search at Scale*. URL: <https://qdrant.tech/>.
- [31] milvus. *Milvus: The High-Performance Vector Database Built for Scale*. URL: <https://milvus.io/>.
- [32] Tensorflow. *glove100 angular dataset*. URL: https://www.tensorflow.org/datasets/catalog/glove100_angular.
- [33] QEMU Project. *QEMU/KVM*. URL: <https://www.qemu.org/>.
- [34] Redis Inc. *redis-py - Python Client for Redis*. URL: <https://redis-py.readthedocs.io/en/stable/>.
- [35] Sean Reifschneider. *python-memcached*. URL: <https://github.com/linsomniac/python-memcached>.
- [36] Jie Liu, Xi Wang, Jianbo Wu, Shuangyan Yang, Jie Ren, Bhanu Shankar, and Dong Li. *Exploring and Evaluating Real-world CXL: Use Cases and System Adoption*. 2024. arXiv: 2405.14209 [cs.PF]. URL: <https://arxiv.org/abs/2405.14209>.
- [37] Yupeng Tang, Ping Zhou, Wenhui Zhang, Henry Hu, Qirui Yang, Hao Xiang, Tongping Liu, Jiaxin Shan, Ruoyun Huang, Cheng Zhao, Cheng Chen, Hui Zhang, Fei Liu, Shuai Zhang, Xiaoning Ding, and Jianjun Chen. "Exploring Performance and Cost Optimization with ASIC-Based CXL Memory". In: *Proceedings of the Nineteenth European Conference on Computer Systems*. EuroSys '24. Athens, Greece: Association for Computing Machinery, 2024, pp. 818–833. ISBN: 9798400704376. DOI: 10.1145/3627703.3650061. URL: <https://doi.org/10.1145/3627703.3650061>.
- [38] Onkar Patil, Latchesar Ionkov, Jason Lee, Frank Mueller, and Michael Lang. "Performance characterization of a DRAM-NVM hybrid memory architecture for HPC applications using intel optane DC persistent memory modules". In: *Proceedings of the International Symposium on Memory Systems*. MEMSYS '19. Washington, District of Columbia, USA: Association for Computing Machinery, 2019, pp. 288–303. ISBN: 9781450372060. DOI: 10.1145/3357526.3357541. URL: <https://doi.org/10.1145/3357526.3357541>.

- [39] Zixuan Wang, Xiao Liu, Jian Yang, Theodore Michailidis, Steven Swanson, and Jishen Zhao. “Characterizing and Modeling Non-Volatile Memory Systems”. In: *2020 53rd Annual IEEE/ACM International Symposium on Microarchitecture (MICRO)*. 2020, pp. 496–508. DOI: 10.1109/MICRO50266.2020.00049.
- [40] Joseph Izraelevitz, Jian Yang, Lu Zhang, Juno Kim, Xiao Liu, Amirsaman Memaripour, Yun Joon Soh, Zixuan Wang, Yi Xu, Subramanya R. Dulloor, Jishen Zhao, and Steven Swanson. *Basic Performance Measurements of the Intel Optane DC Persistent Memory Module*. 2019. arXiv: 1903.05714 [cs.DC]. URL: <https://arxiv.org/abs/1903.05714>.
- [41] Huaicheng Li, Daniel S. Berger, Lisa Hsu, Daniel Ernst, Pantea Zardoshti, Stanko Novakovic, Monish Shah, Samir Rajadnya, Scott Lee, Ishwar Agarwal, Mark D. Hill, Marcus Fontoura, and Ricardo Bianchini. “Pond: CXL-Based Memory Pooling Systems for Cloud Platforms”. In: *Proceedings of the 28th ACM International Conference on Architectural Support for Programming Languages and Operating Systems, Volume 2*. ASPLOS 2023. Vancouver, BC, Canada: Association for Computing Machinery, 2023, pp. 574–587. ISBN: 9781450399166. DOI: 10.1145/3575693.3578835. URL: <https://doi.org/10.1145/3575693.3578835>.
- [42] Philip Levis, Kun Lin, and Amy Tai. “A Case Against CXL Memory Pooling”. In: *Proceedings of the 22nd ACM Workshop on Hot Topics in Networks*. HotNets ’23. Cambridge, MA, USA: Association for Computing Machinery, 2023, pp. 18–24. ISBN: 9798400704154. DOI: 10.1145/3626111.3628195. URL: <https://doi.org/10.1145/3626111.3628195>.
- [43] Qirui Yang, Runyu Jin, Bridget Davis, Devasena Inupakutika, and Ming Zhao. “Performance Evaluation on CXL-enabled Hybrid Memory Pool”. In: *2022 IEEE International Conference on Networking, Architecture and Storage (NAS)*. 2022, pp. 1–5. DOI: 10.1109/NAS55553.2022.9925356.
- [44] Jacob Wahlgren, Maya Gokhale, and Ivy B. Peng. “Evaluating Emerging CXL-enabled Memory Pooling for HPC Systems”. In: *2022 IEEE/ACM Workshop on Memory Centric High Performance Computing (MCHPC)*. IEEE, Nov. 2022. DOI: 10.1109/mchpc56545.2022.00007. URL: <http://dx.doi.org/10.1109/MCHPC56545.2022.00007>.
- [45] Yuhong Zhong, Daniel S. Berger, Carl Waldspurger, Ryan Wee, Ishwar Agarwal, Rajat Agarwal, Frank Hady, Karthik Kumar, Mark D. Hill, Mosharaf Chowdhury, and Asaf Cidon. “Managing Memory Tiers with CXL in Virtualized Environments”. In: *18th USENIX Symposium on Operating Systems Design and Implementation (OSDI 24)*. Santa Clara, CA: USENIX Association, July 2024, pp. 37–56. ISBN: 978-1-939133-40-3. URL: <https://www.usenix.org/conference/osdi24/presentation/zhong-yuhong>.
- [46] Hasan Al Maruf. *Transparent Page Placement for Tiered-Memory*. <https://lore.kernel.org/all/cover.1637778851.git.hasanalmaruf@fb.com/>. [PATCH 0/5]. Linux Kernel Mailing List (LKML), Nov. 2021.
- [47] Daniel S. Berger, Daniel Ernst, Huaicheng Li, Pantea Zardoshti, Monish Shah, Samir Rajadnya, Scott Lee, Lisa Hsu, Ishwar Agarwal, Mark D. Hill, and Ricardo Bianchini. “Design Tradeoffs in CXL-Based Memory Pools for Public Cloud Platforms”. In: *IEEE Micro* 43.2 (2023), pp. 30–38. DOI: 10.1109/MM.2023.3241586.
- [48] Henry N Schuh, Arvind Krishnamurthy, David Culler, Henry M Levy, Luigi Rizzo, Samira Khan, and Brent E Stephens. “CC-NIC: a Cache-Coherent Interface to the NIC”. In: *Proceedings of the 29th ACM International Conference on Architectural Support for Programming Languages and Operating Systems, Volume 1*. 2024, pp. 52–68.
- [49] Mingxing Zhang, Teng Ma, Jinqi Hua, Zheng Liu, Kang Chen, Ning Ding, Fan Du, Jinlei Jiang, Tao Ma, and Yongwei Wu. “Partial Failure Resilient Memory Management System for (CXL-based) Distributed Shared Memory”. In: *Proceedings of the 29th Symposium on Operating Systems Principles*. SOSP ’23. Koblenz, Germany: Association for Computing Machinery, 2023, pp. 658–674. ISBN: 9798400702297. DOI: 10.1145/3600006.3613135. URL: <https://doi.org/10.1145/3600006.3613135>.
- [50] Suyash Mahar, Ehsan Hajyjasini, Seungjin Lee, Zifeng Zhang, Mingyao Shen, and Steven Swanson. *Telepathic Datacenters: Fast RPCs using Shared CXL Memory*. 2024. arXiv: 2408.11325 [cs.DC]. URL: <https://arxiv.org/abs/2408.11325>.
- [51] Jie Zhang, Xuzheng Chen, Yin Zhang, and Zeke Wang. “DmRPC: Disaggregated Memory-aware Datacenter RPC for Data-intensive Applications”. In: *2024 IEEE 40th International Conference on Data Engineering (ICDE)*. IEEE, 2024, pp. 3796–3809.

- [52] Yehonatan Fridman, Suprasad Mutalik Desai, Navneet Singh, Thomas Willhalm, and Gal Oren. *CXL Memory as Persistent Memory for Disaggregated HPC: A Practical Approach*. 2023. arXiv: 2308.10714 [cs.DC]. URL: <https://arxiv.org/abs/2308.10714>.
- [53] Sangjin Lee, Alberto Lerner, Philippe Bonnet, and Philippe Cudré-Mauroux. “Database Kernels: Seamless Integration of Database Systems and Fast Storage via CXL.” In: *CIDR*. 2024.
- [54] Myoungsoo Jung. “Hello bytes, bye blocks: Pcie storage meets compute express link for memory expansion (cxl-ssd)”. In: *Proceedings of the 14th ACM Workshop on Hot Topics in Storage and File Systems*. 2022, pp. 45–51.
- [55] Suyash Mahar, Mingyao Shen, Terence Kelly, and Steven Swanson. “Snapshot: Fast, Userspace Crash Consistency for CXL and PM Using msync”. In: *2023 IEEE 41st International Conference on Computer Design (ICCD)*. 2023, pp. 495–498. DOI: 10.1109/ICCD58817.2023.00082.
- [56] Yi Xu, Suyash Mahar, Ziheng Liu, Mingyao Shen, and Steven Swanson. *CXL Shared Memory Programming: Barely Distributed and Almost Persistent*. 2024. arXiv: 2405.19626 [cs.DC]. URL: <https://arxiv.org/abs/2405.19626>.
- [57] Anthony M Cabrera, Aaron R Young, and Jeffrey S Vetter. “Design and analysis of CXL performance models for tightly-coupled heterogeneous computing”. In: *Proceedings of the 1st International Workshop on Extreme Heterogeneity Solutions*. ExHET ’22. Seoul, Republic of Korea: Association for Computing Machinery, 2022. ISBN: 9781450393447. DOI: 10.1145/3529336.3530817. URL: <https://doi.org/10.1145/3529336.3530817>.
- [58] Adarsh Patil, Vijay Nagarajan, Nikos Nikoleris, and Nicolai Oswald. “Āpta: Fault-tolerant object-granular CXL disaggregated memory for accelerating FaaS”. In: *2023 53rd Annual IEEE/IFIP International Conference on Dependable Systems and Networks (DSN)*. 2023, pp. 201–215. DOI: 10.1109/DSN58367.2023.00030.
- [59] Xingda Wei, Haotian Wang, Tianxia Wang, Rong Chen, Jinyu Gu, Pengfei Zuo, and Haibo Chen. *Transactional Indexes on (RDMA or CXL-based) Disaggregated Memory with Repairable Transaction*. 2023. arXiv: 2308.02501 [cs.DB]. URL: <https://arxiv.org/abs/2308.02501>.
- [60] Angelos Arelakis, Nilesh Shah, Yiannis Nikolakopoulos, and Dimitrios Palyvos-Giannas. *Streamlining CXL Adoption for Hyperscale Efficiency*. 2024. arXiv: 2404.03551 [cs.ET]. URL: <https://arxiv.org/abs/2404.03551>.